Digital Chemical Engineering 14 (2025) 100216

Contents lists available at ScienceDirect

Digital Chemical Engineering

journal homepage: www.elsevier.com/locate/dche

Original Article

A novel CFD-MILP-ANN approach for optimizing sensor placement, number, and source localization in large-scale gas dispersion from unknown locations

Yiming Lang [a], Michelle Xin Yi Ng [a], Kai Xiang Yu [a], Binghui Chen [a,b], Peng Chee Tan [a,b], Khang Wei Tan [a,b], Weng Hoong Lam [a,b], Parthiban Siwayanan [a,b], Kek Seong Kim [a,b], Thomas Shean Yaw Choong [c], Joon Yoon Ten [a,b,*], Zhen Hong Ban [a,b,*]

[a] School of Energy and Chemical Engineering, Xiamen University Malaysia, Sepang, Selangor 43900, Malaysia
[b] College of Chemistry and Chemical Engineering, Xiamen University, Xiamen 361005, China
[c] Faculty of Engineering, Universiti Putra Malaysia, Seri Kembangan, Selangor, 43400, Malaysia

ARTICLE INFO

Keywords:
Source localization
Machine learning
CFD simulation
Optimization
Gas dispersion

ABSTRACT

Illegal practices like open electronic waste incineration release hazardous pollutants, endangering the environment and human health. The Internet of Things (IoT) enables online real-time gas concentrations, but its capability to predict leak sources accurately remains a challenge. A large amount of historical data is required to train the source localization model, as gas dispersion is affected by wind speed and wind direction. Furthermore, sensor placement critically affects precise detection and prediction. This study introduces an innovative approach integrating Computational Fluid Dynamics (CFD), Mixed-Integer Linear Programming (MILP), and Artificial Neural Network modeling (ANN). CFD was utilized for machine learning model training. The MILP was used to optimize sensor placement, while the ANN model was used to optimize sensor number. The source localization model was again realized by the ANN model with optimized sensors data. The trained model was able to identify the unknown illegal electronic waste treatment locations with 97.22 % accuracy in this study. This method allows for the rapid detection of gas sources, as well as the execution of an emergency response, in line with Sustainable Development Goal Target 3.9.

1. Introduction

The advent of the digital age has led to a massive increase in the production and usage of electronic devices in all aspects of human lives and businesses worldwide. However, due to shorter product lifespans, rapid technological advances and increased consumer demand for the latest devices, there has also been a significant increase in electronic waste (e-waste) with approximately 53.6 million tons of e-waste generated globally in 2019 (Forti et al., 2020). Recycling activities have not been able to keep pace with the growth in global e-waste with total amount of e-waste generated exceeding those recycled by 5 times over the same period. In Malaysia, the reported amount of electronic waste produced in 2019 has increased by three times since 2009, reaching around 364 kt (Forti et al., 2020). For industrial e-waste, Malaysia uses the Electronic Scheduled Waste Information System (eSWIS) is used to track e-waste from generation to recycling, with 138 recycling facilities nationwide (Yong et al., 2019). However, household e-waste lacks a similar regulatory framework and is often collected by non-governmental organizations, charities, or individual collectors (Hassan and Shirazi, 2021). Additionally, a lot of electronic waste from overseas is shipped to Malaysia by concealing it as other permitted imports (Bernama, 2022).

E-waste is known to contain heavy metal elements and many organic compounds that can pose environmental and human health risks if not properly disposed of. Consequently, proper treatment and disposal of these large quantities of e-waste have become a concern for many countries globally. Hydrometallurgy is one of the conventional methods used to recover metals from e-waste. It is simpler and requires less capital than electrometallurgy and pyrometallurgy (Neto et al., 2016). Chemicals such as cyanide, nitric acid, and aqua regia (a mixture of nitric and hydrochloric acids) are commonly used to extract some specific metals from e-waste (Gökelma et al., 2016). However, the recovery

* Corresponding authors.
E-mail addresses: joonyoon.ten@xmu.edu.my (J.Y. Ten), bzhong@xmu.edu.my (Z.H. Ban).

https://doi.org/10.1016/j.dche.2024.100216
Received 26 June 2024; Received in revised form 11 December 2024; Accepted 31 December 2024
Available online 2 January 2025

process is usually accompanied by the release of some toxic gases (NO, NOCl, Cl_2, etc.), which requires measures such as well-established exhaust gas treatment devices to ensure the safety and environmental friendliness of formal metal recycling. Improper recycling methods for e-waste are more primitive in some developing countries. Since e-waste contains a significant number of valuable metals, including gold, silver, copper, platinum, etc., many people seek to maximize the profit from illegally recycling these metals (Shumon et al., 2014). One of the main informal recycling methods to separate metals and non-metals is through the open burning of the e-waste without proper gas and liquid treatment (Lu and Xu, 2016; Shahabuddin et al., 2023).

Open-air burning of e-waste can severely impact the environment and human health due to the release of various toxic organic compounds like chlorinated and brominated dioxins and furans, as well as the generation of metallic dusts, such as copper, lead, zinc, and aluminum (Cesaro et al., 2019; Gangwar et al., 2019; Li et al., 2018; Sahle-Demessie et al., 2017). These toxic substances can cause extensive environmental pollution through atmospheric dispersion and deposition into soils and waters. They could accumulate in living organisms and enter the food chain, which can cause long-term hazards to biological and human health. Several studies have shown an increased risk of cardiovascular disease and cancer for the residents living near e-waste recycling sites that were caused by long-term exposure to heavy metals (Davis and Garb, 2019; Gangwar et al., 2019; Huang et al., 2016; Zheng et al., 2013). Therefore, reducing the illegal behavior of e-waste open burning is vital for both the health of the residents and the ecosystem.

The fast detection and subsequent deployment of quick and effective response against illegal e-waste open burning can minimize the risks towards human health. A smart detection or monitoring system is a solution that may help detect hazardous gas and stop or prevent accidents by working with little or no human supervision. Devices with Internet-of-Things (IoT) capabilities are commonly employed by such systems to ensure real-time monitoring and alert operators in case of abnormalities. One major issue in the development of smart systems is the proper amount and placement of IoT-based sensors. Sensor layout optimization can shorten detection time, reduce energy and maintenance costs, as well as maximize risk mitigation. The performance of a sensor network relies on the placement and number of sensors, which are determined based on various parameters including release location, type of fluid released, operating conditions, geometry of the plant, and meteorological conditions. An increase in the number of sensors can improve the detection performance, but an overabundance of sensors can lead to higher costs as well as an increase in the number of false alarms. The placement of sensors is also vital in avoiding false alarms and blind spots. The standard approach to sensor layout placement is via qualitative methods, typically arising from rule of thumbs and engineering experience, which can subjective and biased (Cen et al., 2018; Rad et al., 2016). One common method is to place sensors uniformly within the monitoring space, resulting in a large number of sensors and an expensive monitoring system (Fontanini et al., 2016). Sensor deployment through these methods often fails to maximize performance to identify the gas dispersion sources accurately.

Quantitative methods, which are objective and measurable, may serve as substitutes or supplements to current qualitative methods. For hazardous contaminant detection, quantitative values include concentration and volume of fluid. Quantitative models organize and interpret the measured datasets using mathematical equations to recognize specific patterns and trends for a particular problem. To optimize sensor placement, the mixed-integer linear programming (MILP) heuristics-based technique is commonly used and has been verified for a variety of applications by utilizing the quantitative data to solve for mathematical optimization problems. This technique integrates both continuous and discrete variables and accurately models the constraints present in the real world, making it able to handle discrete variables as well as incorporate multiple constraints and objectives needed for sensor optimization. Legg et al. (2012) utilized the MILP technique to identify the best locations for gas detectors in petrochemical facilities, and they were able to achieve computational efficiency within seconds. Similarly, Klise et al. (2020) showed how the MILP technique can be used to identify the best sensor locations and detection thresholds for optimal detection of emission scenarios in methane emission settings. An improved MILP based on the work by Legg et al. (2012) was presented by Benavides-Serrano et al. (2015) with the inclusion of unavailability and voting effects (SP-UV) to account for potential false negatives and false positive alarms. Results indicated that the SP-UV technique was able to achieve an expected time to detection that was 30 s or less than industry common methodologies such as Random Approach (RA), Volumetric Approach (VA), Minimum Source Distance Problem (MSDP), Greedy Coverage (GC) and the Maximum Coverage Location Problem (MCLP) formulation. Compared to installing sensors around the facility or in individual locations, an optimized sensor network yields consistent improvement in detecting leaks. The use of MILP in optimizing sensor placement enhances efficiency and cost-effectiveness in various scenarios. However, an optimized sensor layout can only detect possible leakages and offer information on the concentration of hazardous fluid in the surrounding location of the sensors of interest. An optimized sensor layout alone cannot analyse the obtained information nor help in source tracking or localization to find the leakage points in a smart system. Further quantitative analysis through numerical or computational methods is common to understand the dispersion behaviour of hazardous fluid away from the source in the event of open burning or accidental release.

Due to the complexities in urban dispersion modelling including environmental conditions, obstacle presence, and terrain effects, computational models are being utilized to predict and offer insights into pollution transport (Boikos et al., 2024; Ioannidis et al., 2024; Lyu et al., 2023). These models can be utilized to assist authorities in analysis of open burning operations and pollution control to help decrease environmental damage and protect human health. Among the various models, Computational Fluid Dynamics (CFD) is a powerful tool for studying air dispersion with varying time in a complex geographic system. It can be used to obtain data for real-world scenarios that are difficult or costly to obtain, such as smoke dispersion in fires and toxic gas leaks in chemical plants (Baalisampang et al., 2021; Chen et al., 2022). However, when the source of the gas release is unknown, the use of CFD models alone is limited. In addition, CFD modelling and calculations along with data analysis are time-consuming, which limits the application of CFD in emergency and contingency situations. Powerful data analysis tools are required to analyse the diverse and large amounts of numerical data (big data) and assist in the determination of source location through by recognizing specific patterns and trends. Therefore, in complex source localization problems, the combination of CFD with other data analysis techniques can be useful in predicting the location of the release point in a shorter period of time.

Probability-based source estimation algorithms such as the inverse Markov chain Monte Carlo (MCMC) sampling method based on Bayesian inference have been combined with a high-resolution CFD model for source localization was used to predict the source of the steady-state pollutant plume in complex urban geometry results in a study by Chow et al. (2005) through forward advection-diffusion equation calculations. The prediction of the concentration plume by the CFD code in this study was inadequate and there was some difficulty in source location prediction when it was between two buildings perpendicular to the flow direction. Moreover, the computational resources for the forward advection-diffusion equation are intensive as the equation is solved for every combination of the source parameter or source locations, which can reach a considerably large number. To optimize the computational efforts required for steady-state source estimation, Keats et al. (2006) and Keats et al. (2007) utilized same inverse MCMC sampling method to solve the advection-diffusion equation with the adjoint approach. This led to the linear scaling of computational resources with the number of detectors and source parameters, instead of scaling

linearly with number of potential source locations and exponentially with the number of source parameters, which would typically be much larger in number compared to the limited number of detectors. As the computational time for solving the adjoint advection-diffusion equation once is similar to the forward advection-diffusion equation, the total computational resources required can be cut short. In a study by Zeng et al. (2020), an inverse Markov chain-based method that is able to identify pollutant source locations in buildings with ventilation systems with complete and incomplete prior concentration distribution was developed to provide fast source inversion modelling with low computational load. Through the validation by CFD simulation and concentration measurement experiments based on instantaneous release, this Markov chain approach was able to achieve the correct prediction of the source, though additional research may be needed for the localization of continuous release sources. Furthermore, the placement of detectors in this study was found to have impacted the results of the source localization, wherein placing detectors in well-mixed zones. This was similar to the findings by Wu et al. (2020) involving a study utilizing combined CFD-Bayesian inference method for source term estimation, which tested layouts of sensors were set to intervals of 10 m, 20 m, and 30 m and found the increasing number of sensors were shown to improve unknown source localization accuracy. This aligns with the purpose of sensor placement optimization via quantitative analysis as sensors are major components for supplying models the relevant and accurate data for source localization purposes.

There is also the issue of computational resources for probability-based algorithms source localization, which can be minimized by inclusion of optimization techniques. As a metaheuristic method, GA has already been applied as an optimization algorithm to optimize sensor placement and has been extensively studied for source localization. The location of the source is confirmed by applying specific functions and iterations to find the minimum gap between the calculated and detected concentrations. Haupt et al. (2006) presented the usage of a GA-coupled Monte Carlo method with a basic Gaussian plume dispersion model for source characterization including the strength, location, and time of the release. The Monte Carlo method was used to analyse the error bounds associated with the ability of the GA model to match a known solution based on the previously mentioned three characteristics. In a separate paper with the same coupled method, Haupt et al. (2007) studied the prediction of the release of toxic pollutants, and applied GA to characterize the two-dimensional source location, release amount, and wind direction. Compared with the random search method, the GA achieved convergence faster and was able to deal with more complex situations. In research by Allen et al. (2007), a similar GA-coupled approach with a Gaussian plume dispersion model was used to find the 2D source information by obtaining the output data of the dispersion model with the best match for the receptor data. After 100 iterations, the algorithm can effectively reproduce the source information including source location, source intensity, and wind direction. Annunzio et al. (2012) combined GA with a hybrid Langrangian-Eulerian framework for the backtracking of discrete particles to determine the average state of the dispersion of contaminants and utilize this information for the prediction of the 2D source location. Cantelli et al. (2015) managed to achieve 3D source location identification by applying GA on the obtained pollutant concentrations measured by fixed sensor positions as simulated using a Gaussian model. However, the source characterization conducted in the above studies were commonly based on simple geometries or releases at ground level with flat terrain. For complex terrain, additional parameters must be considered including meteorological conditions and the dispersion of wind and contaminant fluid flow when encountering the associated obstacles as the dispersion model is critical in determining accurate sensor readings for source localization purposes. Furthermore, the Gaussian dispersion model is used in many of the aforementioned studies mostly due to its computational efficiency. The Gaussian dispersion model assumes the dispersion of the plume is normally distributed in the downwind direction and there is some difficulty for the model to predict accurate concentrations in complex environments as well as maintain performance with increasing number of random inputs (Holmes and Morawska, 2006). For more complex scenarios, alternative methods have been employed for source localization such as CFD, as aforementioned, for forward dispersion modelling and data-driven models for dispersion data analysis and prediction of accurate concentration in complex systems.

With Artificial Intelligence (AI) to play a pivotal role in the development of smart systems and solutions in the future, data-driven and learning-based AI, called machine learning (ML) has enormous potential in streamlining the CFD data analysis process. Introduction of ML has the potential to obtain more accurate source location predictions. Ma et al. (2021) utilized a combined Gaussian-support vector machine (SVM) leaning dispersion algorithm with the Markov chain Monte Carlo method and found that the inclusion of the ML algorithm into the MCMC method resulted in closer convergence to the actual pollutant source compared to the non-ML MCMC-Gaussian method. The Artificial Neural Network (ANN) is an example of an artificial intelligence-based quantitative model that is able to learn from experience or data, identify patterns, and make decisions without human intervention (Xu et al., 2021b). To date, several studies have been conducted to utilize machine learning techniques in source localization due to its ability to find patterns quickly in large amounts of data. ANNs have shown potential in source localization, as evidenced by several studies. Zhou and Tartakovsky (2021) integrated a deep convolutional neural network (CNN) to mitigate the high computational costs commonly associated with the MCMC method when using the forward transport model. The MCMC-CNN method reached the predicted solution 20 times faster due to the usage of the GPU, rather than the CPU as typically utilized by partial differential equation (PDE) solvers in the previous literature. This improvement in computational time is important, especially for simulations involving more complex dispersion in complicated geometries. Moreover, the integration of the CNN provided comparable results in terms of the source location, spread, and strength to the non-CNN model as well as allowed for the quantification of predictive uncertainty and was able to account for measurement errors. ML-coupled methods are fast and also sufficiently accurate in terms of source characterization. In a study of groundwater contamination sources, researchers trained a feed-forward three-level ANN model to estimate the concentrations and locations of source contaminants (Chaubey and Srivastava, 2020). The researchers trained the ANN model using 1500 data sets, and the resulting neural network, with a 22-16-2 architecture, achieved the best identification with an NRMSE of just 0.014. In a previous report, the release of toxic gases (methane and benzene) resulting from the open burning of plastics was investigated using CFD-ANN models (Yu et al., 2022). To perform source localization, the ANN model was trained using 65 sets of concentration profiles obtained from CFD simulations. The ANN model identified 12 possible release points using 8 sensors, with an 85.71 % validation rate and an average error of 3.86 %. Furthermore, ANN-based models have been utilized for source localization in more complex environments containing obstacles or complex terrain. Xu et al. (2021a) compared ANN and Convolutional Neural Networks (CNN) for toxic gas source localization with obstacles, finding ANN better for source location prediction and CNN superior in source term precision. Chen et al. (2022) used CNN to locate leaks and wind direction in a chemical park with various buildings, achieving over 99 % accuracy due to CNN's high spatial feature extraction capability. Cho et al. (2018) implemented Deep Neural Networks (DNN) for chemical plant leak localization, achieving about 75.43 % accuracy with 25 hidden layers. Kim et al. (2019) used Recurrent Neural Networks (RNN) with Long Short-Term Memory cells for leak source localization, achieving 97.08 % accuracy using CFD simulation data obtained from fixed type sensors for training. Thus, the utilization of neural networks has the potential to provide fast and accurate source localization for complex systems unlike GA-based models in previous studies which focused more on flat terrain without obstacles.

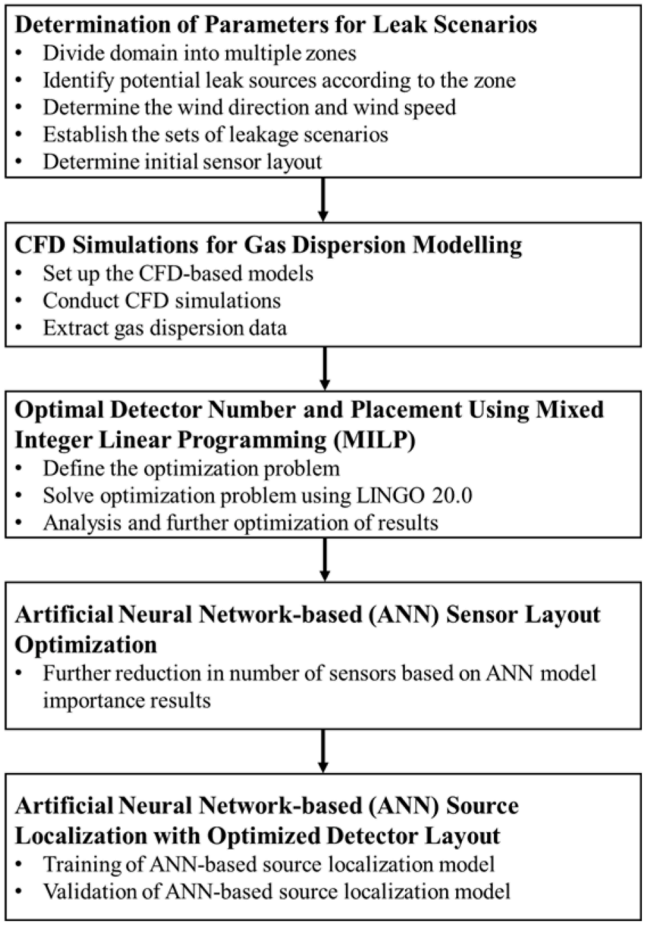

Fig. 1. The framework of the CFD-ANN source localization model.

Table 1
Statistics of the generated industrial e-waste in different States of Malaysia in 2017 (Yong et al., 2019).

State	Generation of industrial e-waste (tones)	State	Generation of industrial e-waste (tones)
Pulau Pinang	48,931.6	Kelantan	294.56
Selangor	14,580.6	Sabah	140.44
Sarawak	3261.16	Kuala Lumpur	120.46
Johor	3008.63	Pahang	87.07
Melaka	2537.09	Terengganu	43.12
Negeri Sembilan	2287.15	Labuan	32.49
Kedah	928.14	Putrajaya	20.39
Perak	593.87	Perlis	18.95

To date, effective methods for detection and source localization remain limited. Thus, it is challenging to effectively prohibit illegal open-burning sites. Besides, effective sensor placement is another challenge in obtaining representative data. Due to practical constraints, it is often not feasible to deploy sensors over an entire area; therefore, sensors are usually placed near known sources. The large number of sensors required makes the implementation practical but not feasible. The proposed method overcomes the shortcomings of the existing approach. This study employs a combination of computational fluid dynamics (CFD), mixed-integer linear programming (MILP), and artificial neural network modeling (ANN) to optimize sensor deployment and number and localize unknown burning sites arising from open burning of e-waste. For the CFD simulation, a domain of 3 km x 3 km with multiple buildings and terrains was selected. A total of 108 CFD simulations were conducted to train the machine learning model with various dispersion scenarios including different wind speeds and directions, with the presence of buildings and terrain as obstacles.

The fast source identification model allows the authorities to stop the burning behavior at the source before the toxic gases are continuously released into the environment and to design an effective emergency plan. This method is also expected to assist the world in embracing the World Health Organization (WHO) Sustainable Development Goal Target 3.9, which is to reduce the number of deaths and illnesses from hazardous chemicals and air pollution.

2. Numerical method

The dispersion of toxic components in the air was simulated using the Computational Fluid Dynamics (CFD) approach. The ANSYS Academic Research FLUENT software was utilized for the purpose of simulation. This study focused on copper, a frequently found heavy metal element in e-waste and a major hazardous component generated during the combustion of e-waste. During the simulation, the dispersion of copper particles under varying wind conditions resulting from open burning was investigated. The domain of the current work is considerably large and thus, experiment work was not conducted. However, the CFD results in the current work was obtained using well validated software, ANSYS FLUENT, which was used in various similar studies involving particle dispersion in the air in hilly areas and in complex urban environments (Du et al., 2021; Fernández-Pacheco et al., 2023).

The framework of the proposed methodology for the development of the source localization model is shown in Fig. 1. First, the domain was divided into uniform zones where each has a designated leak source location. The sets of leakage scenarios were established based on the leak source locations and possible meteorological conditions of the domain. A preliminary sensor layout was deployed through uniform sensor placement. The sets of leakage scenarios were simulated using CFD-based models and the gas concentration data in the form of copper particle concentration plots were collected. With the dispersion information, the MILP optimization problem based on the copper particle damage coefficient and minimization of number of sensors was solved using LINGO 20.0. After analysis and further optimization, the optimal sensor layout was deployed for source localization purposes. The training and validation of the ANN-based source localization model was conducted to determine the accuracy and error. Additional reduction in the number of sensors was performed based on the sensor importance results to further save costs.

2.1. Computational domain

Penang, one of Malaysia's most urbanized and industrialized cities, is home to numerous electronic factories and a large residential population. E-waste recycling data presented in Table 1 indicate that Pulau Pinang (Penang) has the highest amount of e-waste recycled in the formal industrial e-waste recycling system in Malaysia. However, latest news reports have revealed that the Ministry of Environment intercepted a shipment of electronic waste from the US disguised as "Aluminum alloy" in Penang (Bernama, 2022). Therefore, Penang Island was selected as the site of interest in this study.

After conducting a preliminary study of the topography and locations, a specific 3 km × 3 km rhombus-shaped simulation region was chosen for this study. This region is in the southwest of Penang International Airport, adjacent to the residential area of Teluk Kumbar, and approximately 5 km from the Bayan Lepas Free Industrial Zone, home to many electronic equipment manufacturing factories. The selected simulation area comprises part of the coast and sea, part of the mountains, and part of the residential buildings. A map of the study area is shown in Fig. 2.

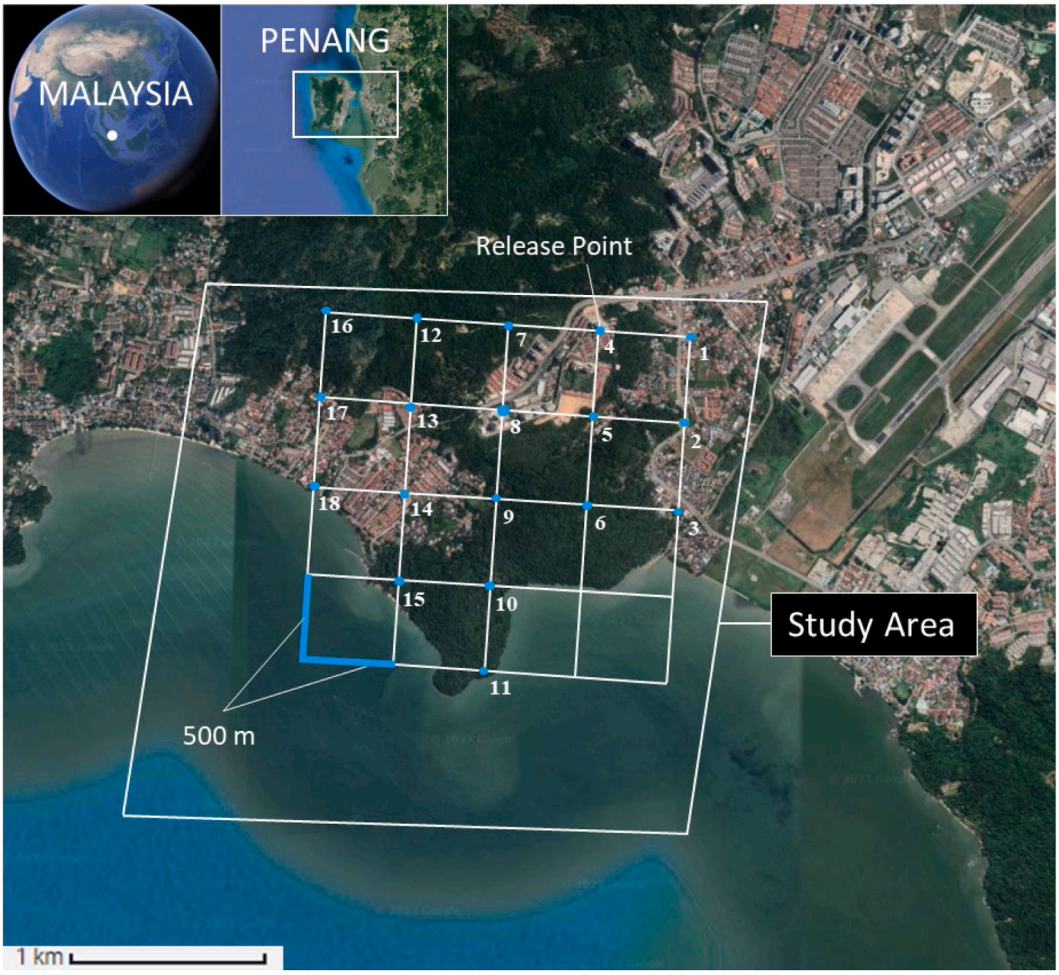

Fig. 2. The study area in Penang, Malaysia.

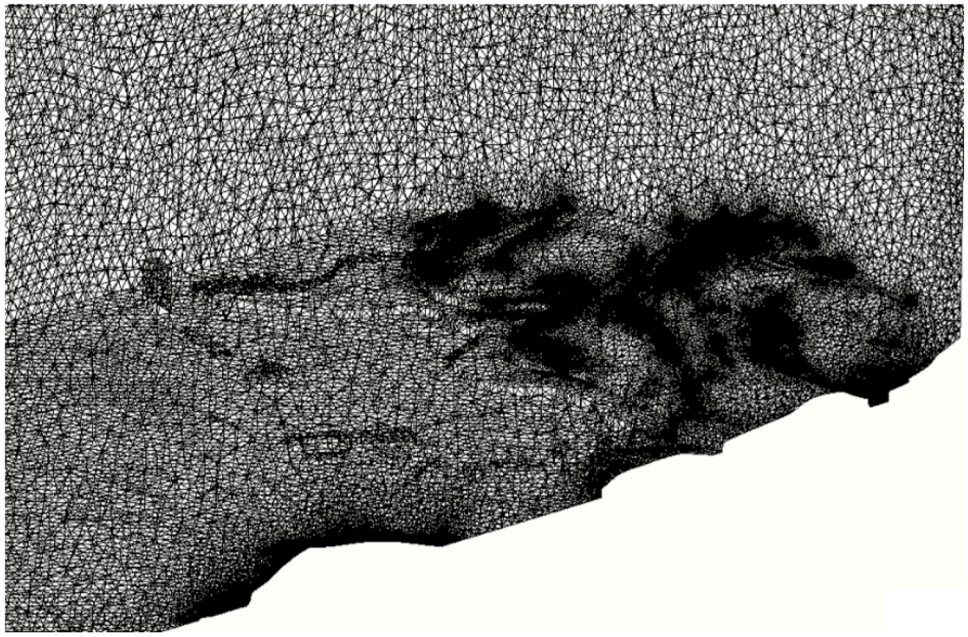

Fig. 3. Mesh of a section of the mountainous area.

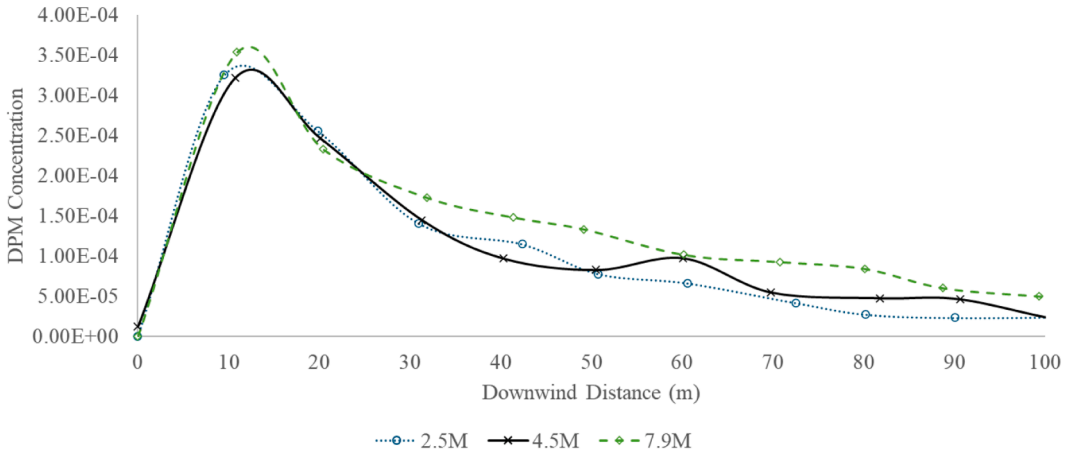

Fig. 4. The copper particle concentration at a height of 50 m for points at an interval of 10 m up to 100 m downwind release from Point 9 with 1.6 m/s east wind.

Table 2
Boundary conditions.

Particle	Copper
Size	5 μm
Release rate	0.0972 kg/s
Initial rise velocity	5 m/s
Wind speed	1.6 m/s, 3.4 m/s, 5.5 m/s
Wind direction	East & West

Table 3
Conditions of validation sets.

Release Locations	Point 1 to Point 18 (18 points)
Wind speed	2.5 m/s or 4.5 m/s
Wind direction	East and West

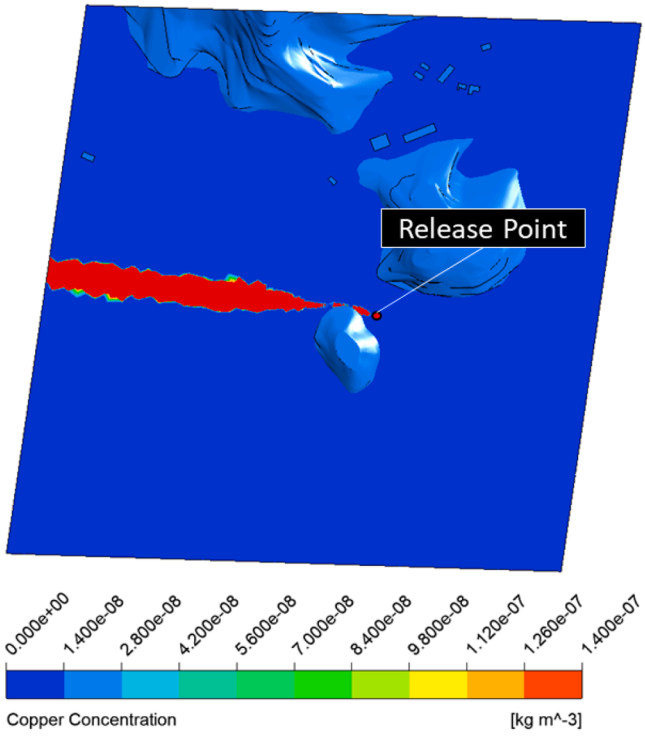

Fig. 5. Case 55: Point 10, 1.6 m/s east-wind.

Since the burning point is unknown, it was decided that18 release points for CFD simulation were selected, with each point located 500 m apart. The dispersion of copper particles will be simulated multiple times for each point, wherein each was subjected to different boundary conditions.

The presence of obstacles has a notable impact on fluid behavior in CFD simulations. This study acknowledges this issue and, to achieve a more accurate depiction of gas dispersion in the chosen region, mountains and buildings were integrated into the geometric model. Geographic information, required for this modeling, was obtained from OpenStreetMap (OpenStreetMap, 2018).

The mesh used in the study consisted of around 4.56 M elements with 850 K nodes and all cells were tetrahedral cells. A mesh of a section of the mountainous area can be seen in Fig. 3.

A grid-sensitivity study or mesh independence study was conducted using three different grid resolutions, which are 2.5, 4.5 and 7.9 million cells. The leak scenario consisting of release position P9 with release velocity of 5 m/s and wind velocity of 1.6 m/s was chosen to check grid independence. As illustrated in Fig. 4, the three grid resolutions are relatively consistent with one another. Thus, the 4.5 million cells grid was chosen to model the dispersion of copper particles as it was deemed a balance between computational resources and simulation accuracy.

2.2. Governing equation

The continuity equation and momentum equation shown below are the governing equations for this study. Given the low level of impact, thermal effects will not be considered, and no reactions are anticipated.

Continuity equation:

$$\frac{\partial \rho}{\partial t} + \nabla \cdot \left(\rho \vec{V}\right) = 0 \tag{1}$$

Momentum Equation: x – component:

$$\frac{\partial(\rho u)}{\partial t} + \nabla \cdot \left(\rho u \vec{V}\right) = -\frac{\partial p}{\partial x} + \frac{\partial \tau_{xx}}{\partial x} + \frac{\partial \tau_{yx}}{\partial y} + \frac{\partial \tau_{zx}}{\partial z} + \rho f_x \tag{2}$$

y – component:

$$\frac{\partial(\rho v)}{\partial t} + \nabla \cdot \left(\rho v \vec{V}\right) = -\frac{\partial p}{\partial y} + \frac{\partial \tau_{xy}}{\partial x} + \frac{\partial \tau_{yy}}{\partial y} + \frac{\partial \tau_{zy}}{\partial z} + \rho f_y \tag{3}$$

z – component:

$$\frac{\partial(\rho w)}{\partial t} + \nabla \cdot \left(\rho w \vec{V}\right) = -\frac{\partial p}{\partial z} + \frac{\partial \tau_{xz}}{\partial x} + \frac{\partial \tau_{yz}}{\partial y} + \frac{\partial \tau_{zz}}{\partial z} + \rho f_z \tag{4}$$

Where, ρ is the density of the fluid; t is time; $\vec{V}$ is the velocity vector; u, v

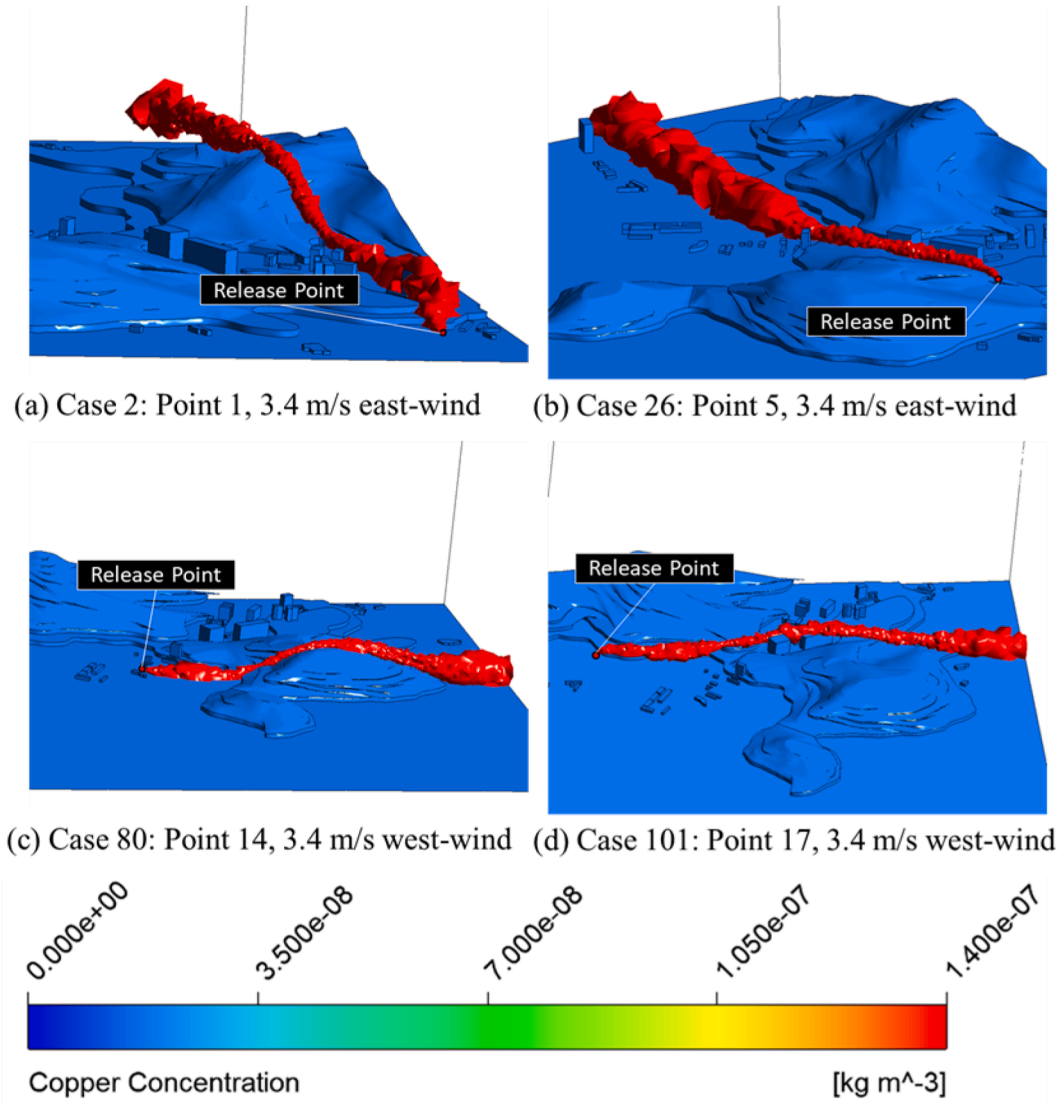

Fig. 6. Terrain effects in case 2, 26, 80 and 101 with 1.4×10^{-7} kg/m^3 isosurface copper particles.

and w are the velocity component in x, y and z direction respectively; τ is the component of the stress tensor; f is the body force per unit mass in each direction.

The Discrete Phase Model (DPM) is a widely used computational fluid dynamics simulation technique used to analyze the behavior of dispersed particles or droplets in a fluid flow. DPM is a framework that tracks the motion and interactions of individual discrete phases, allowing for the analysis of various phenomena, such as particle dispersion, deposition, and coalescence. For example, the use of a coupled CFD simulation and the DPM approach can be used to predict particle deposition in horizontal gas flows and is validated by experimental data (Stone et al., 2019). The DPM is efficiently applied to track individual particles in the fluid flow, accurately simulating their trajectories and deposition patterns. The method demonstrates a strong correlation between simulated and observed results, highlighting its reliability and adaptability to a wide range of particle sizes and flow conditions. The effectiveness of the DPM method lies in its ability to provide accurate predictions and valuable insights for optimizing industrial processes involving particulate matter. Therefore, the DPM method was utilized to simulate the dispersion of copper particles in air. The governing equation for DPM in ANSYS FLUENT is described as (ANSYS, 2020):

$$m_p \frac{d\vec{u}_P}{dt} = m_p \frac{\vec{u} - \vec{u}_P}{\tau_r} + m_p \frac{\vec{g}(\rho_p - \rho)}{\rho_p} + \vec{F} \tag{5}$$

where m_p is the particle mass, $\vec{u}$ and $\vec{u}_P$ are the velocities of the fluid phase and the particle respectively, ρ is the fluid density, ρ_p is the density of the particle, $\vec{F}$ is an additional force, $m_p \frac{\vec{u} - \vec{u}_P}{\tau_r}$ is the drag force, and τ_r is the droplet or particle relaxation time calculated by:

$$\tau_r = \frac{\rho_p d_p^2}{18\mu} \frac{24}{C_d Re} \tag{6}$$

Here, μ is the molecular viscosity of the fluid, d_p is the particle diameter, and Re is the relative Reynolds number.

2.3. Boundary condition

The dispersion of gases in outdoor environments is significantly impacted by release rate, release point, wind speed, and wind direction. This study investigates the impact of varied wind speed and direction, as well as the location of the burning sites. Wind speeds of 1.6 m/s, 3.4 m/s, and 5.5 m/s were selected based on average, maximum, and minimum wind speeds recorded in Penang International Airport in 2021

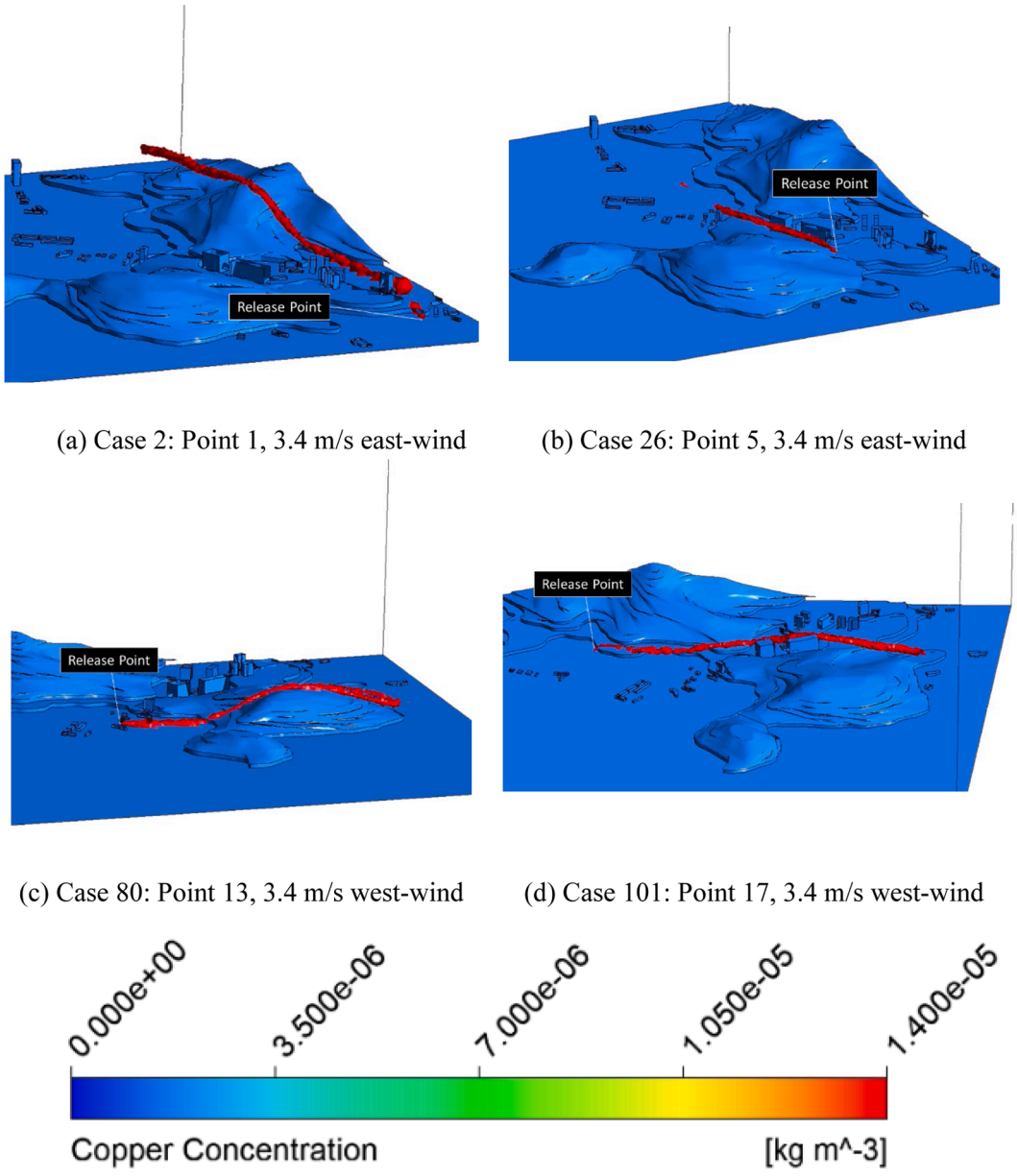

Fig. 7. Terrain effects in case 2, 26, 80 and 101 with 1.4 × 10^{-5} kg/m^3 isosurface copper particles.

(Meteoblue, 2022). The most frequently observed wind directions in Penang, East and West, were also included in the study. The atmosphere class was assumed to be stable (Pasquill Stability Class E) with negligible vertical thermal gradient variation, thereby the impact of vertical thermal gradient was not considered. In this current work, the scope was limited to the stable atmosphere only as the focus is primarily on the development of the coupled method of CFD, MILP, and ANN for sensor placement optimization and source localization. Further work will be considered to improve the accuracy of the model by simulating various atmospheric stability classes. In regard to the buoyancy effects from the burning source, it was considered that the thermal gradient is more obvious closer to the source. When taking into account the overall dispersion over long distances, the influence of the burning source is compared to the influence of the wind speed, which dominates over long distances (Liu and Wen, 2002).

In order to simulate the release of copper particles during the combustion of e-waste, the release point was preset as a circular plane with a diameter of 4 m and a height of 3 m above the ground. Based on the literature, it was deduced that the release percentage of copper during the combustion of e-waste was in the range of 0.056–0.111 kg/s (Cesaro et al., 2019). In contrast, Achtemeier et al. (2011) showed that the initial plume velocity of the smoke released by combustion ranged from 5 m/s to 15 m/s. Şahin et al. (2012) analyzed the particle size of copper particles in air and found that the most common particle distribution was mainly in the range of 3.3–5.8 μm. Therefore, in this study, the release velocity of copper particles was assumed to be 0.0972 kg/s and to rise vertically with a velocity of 5 m/s. For the constant release rate, fluid release and dispersion have been found to use constant release rates (Kontos et al., 2022; Zheng and Chen, 2010). The particle size of copper was set at 5 μm. A summary of the boundary conditions is presented in Table 2.

A total of 18 release points will be simulated in this study, with each point individually evaluated for dispersion under three distinct wind speeds and two wind directions, resulting in 108 simulations. These 108 scenarios will be employed for optimizing sensor placement as well as training artificial neural network models. Furthermore, to ensure the validity and accuracy of the trained model, an additional 36 data sets will be simulated at wind speeds of 2.5 and 4.5 m/s and used as

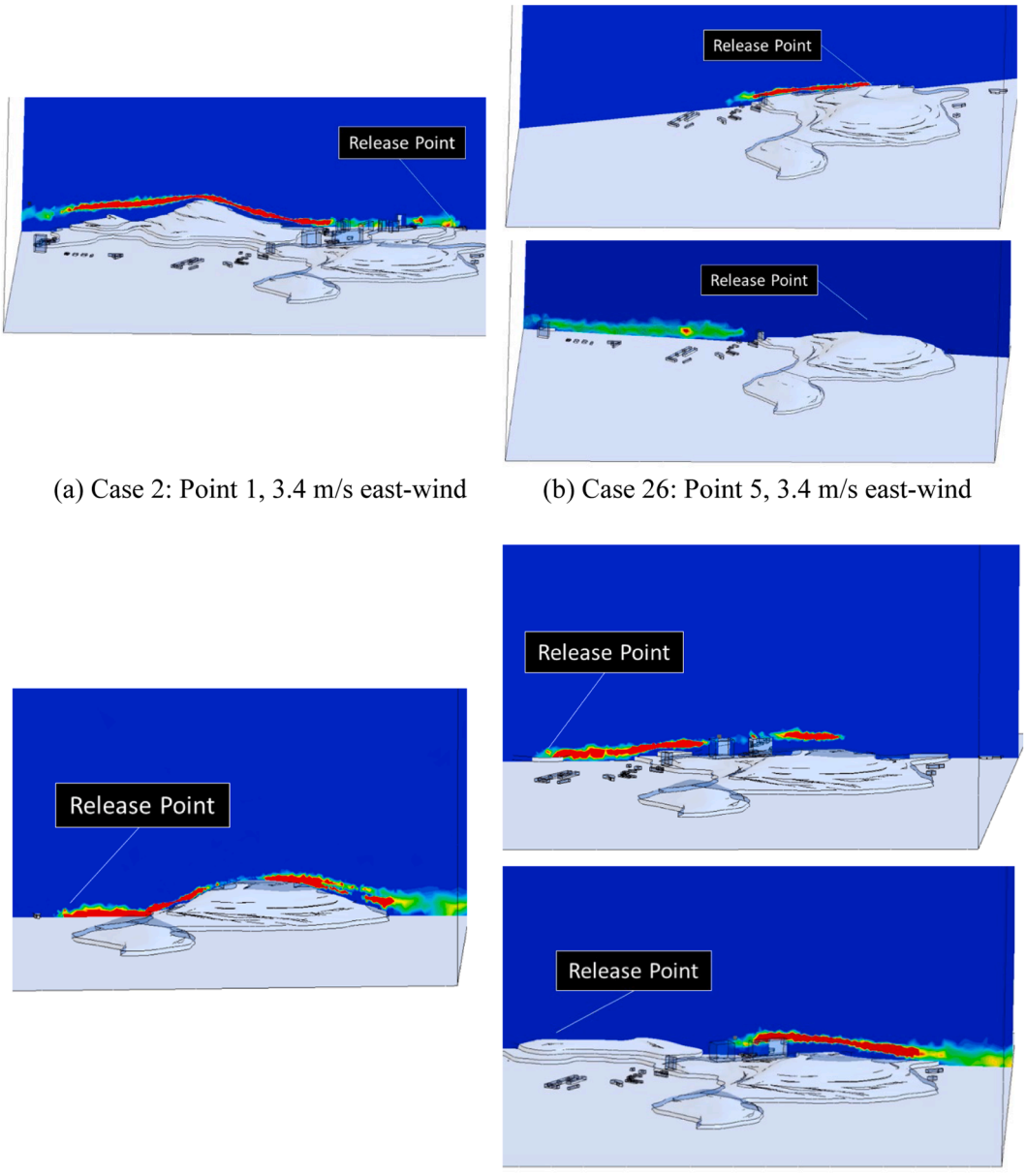

(a) Case 2: Point 1, 3.4 m/s east-wind (b) Case 26: Point 5, 3.4 m/s east-wind

(c) Case 80: Point 13, 3.4 m/s west-wind (d) Case 101: Point 17, 3.4 m/s west-wind

Fig. 8. Terrain effects in case 2, 26, 80 and 101 with 0 to 1.4 $\times$ 10^{-5} kg/m^3 contour plot copper particles.

validation data (Table 3).

2.4. Sensor optimization

The MILP formulation for gas sensor placement optimization is described as below,

$$\max \sum_{i \in I} Z_i \sum_{j \in J} d_{i,j} x_{i,j} \tag{7}$$

subject to

$$\sum_{j \in J} y_j \leq p \tag{8}$$

$$x_{i,j} \leq y_j \; \forall \, i \in I, j \in J \tag{9}$$

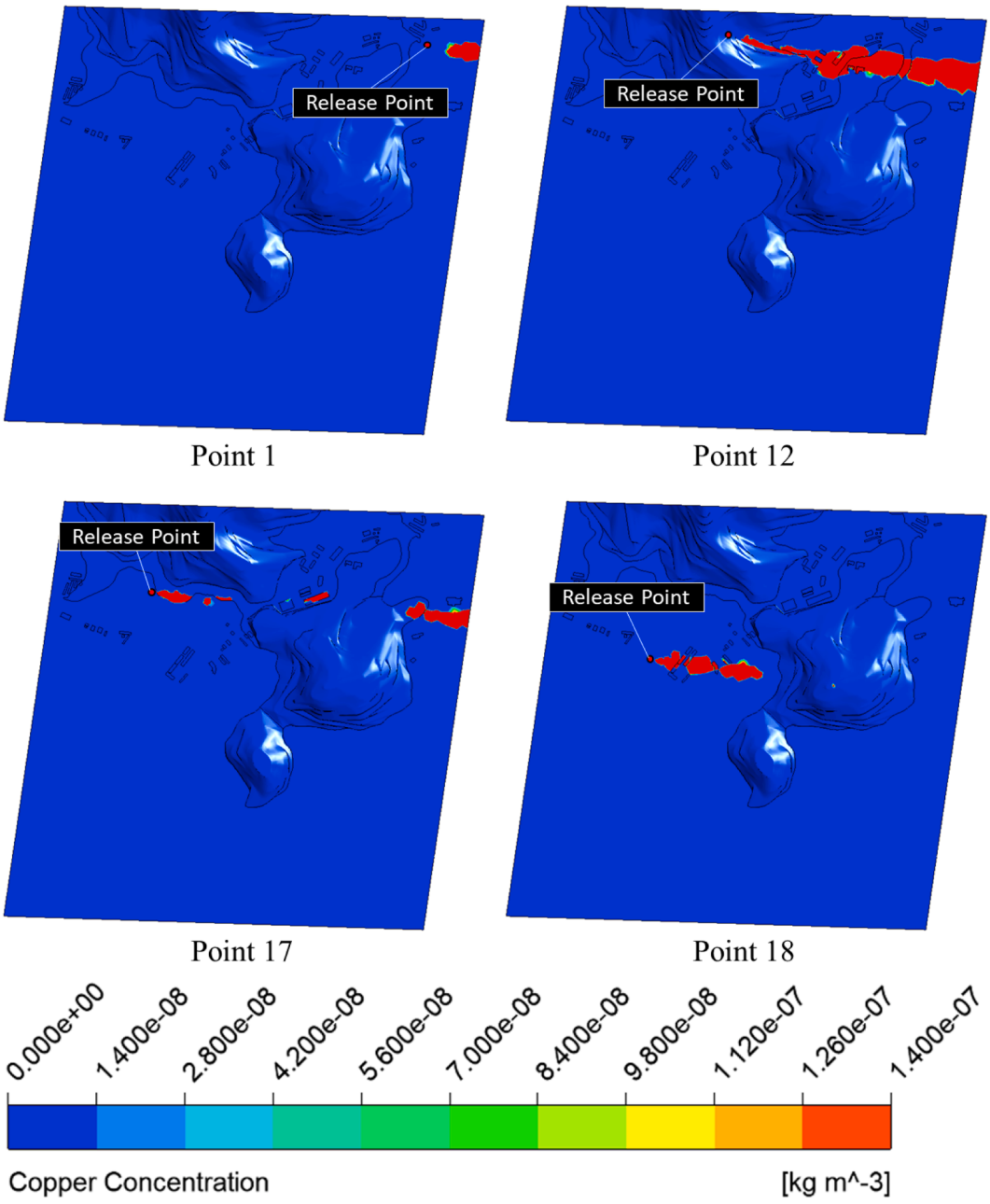

Fig. 9. Dispersion profiles at release point 1, 12, 17 and 18 under 3.4 m/s west-wind.

$$\sum_{j \in J} x_{i,j} = 1 \; \forall \, i \in I \tag{10}$$

$$y_j \in \{0,1\} \; \forall \, j \in J \tag{11}$$

$$x_{i,j} \in \{0,1\} \; \forall \, i \in I, j \in J \tag{12}$$

Where, i is the set of release scenarios, indexed by I; j is the set of candidate sensor locations, indexed by j; Z_i is the occurrence probability of release scenario i; $d_{i,j}$ is the damage coefficient for release scenarios i at location j; $x_{i,j}$ is the indicator of location j is the highest concentration for scenario i; y_j indicating if a sensor is installed at monitoring point j; p is the maximum quantity of gas sensor.

The objective function in Eq. (7) is to maximize the damage coefficient, $d_{i,j,}$ associated with the detected release using a limited number of sensors. The damage coefficient, in this study, is the copper particle concentration present in the domain measured by the sensor network as obtained from CFD simulations. As the number of sensors increase, it is expected that the total copper particle concentration measured by the network also increases until all the copper particle concentration has been measured, which suggests that the sensor network has reached maximum coverage. The maximization of sensor network coverage area is one of the key goals of sensor layout optimization (Karatas, 2020; Yakıcı and Karatas, 2021). By quantifying the coverage area using total copper particle concentration, the model is able to determine the optimal sensor count needed, thereby saving costs without compromising too much on performance.

The probability of each release scenario occurring is assumed to be the same in this work, i.e. the Zi coefficients are assumed to be 1. The concentration of copper particles detected by the sensor is a primary factor affecting the damage coefficient, $d_{i,j}$. Eq. (8) limits the number of sensors and ensures that the number can be optimized to the minimum. In Eq. (11), y_j is equal to 1 only when the sensor is at position j, and 0 otherwise. In Eq. (12), The parameter $x_{i,j}$ is defined as 1 when position

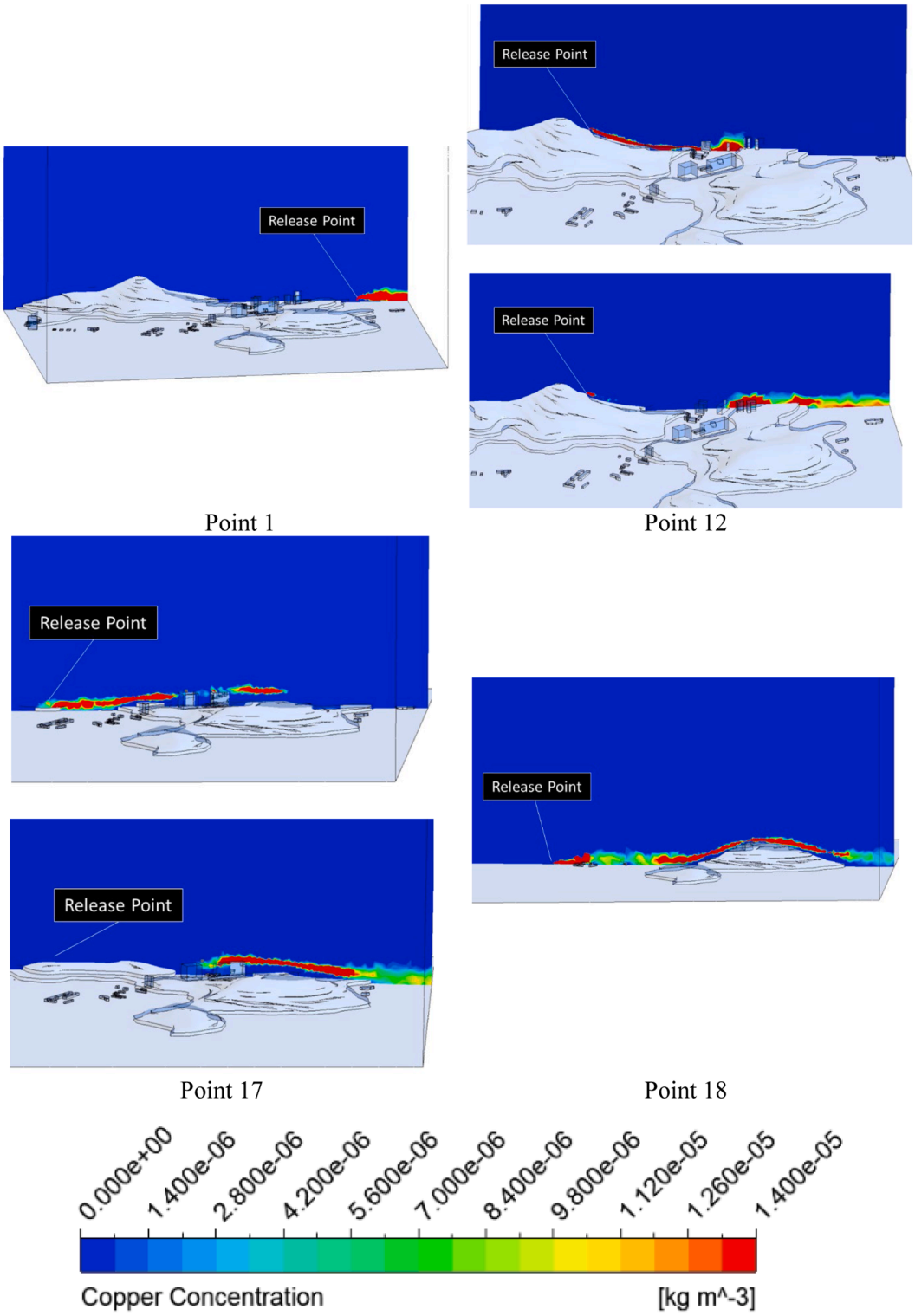

Fig. 10. Copper concentration contour plots under 1.4×10^{-5} kg/m^3 for cases of release points 1, 12, 17 and 18 under 3.4 m/s west-wind.

j is the highest concentration in case i, and 0 otherwise. Eq. (9) ensures that there is a sensor placed at the location j with the highest concentration in case i. Eq. (10) ensures that each case has at least one sensor used to detect the concentration at its location j. The maximum number of sensors will be tested and adjusted until the damage coefficient reaches its maximum.

To solve the MILP problem, LINGO 20.0 software (Educational License) was utilized. This software is well-suited for modeling and solving complex linear, nonlinear, and integer programming problems across a variety of industries. Previous studies by Opit et al. (2021) and Zhou (2021) have demonstrated the efficacy of LINGO software in optimizing sensor placement and network deployment using MILP models. From these studies, it can be concluded that the LINGO software, as a lightweight and programmable optimization software, performs well in MILP optimization.

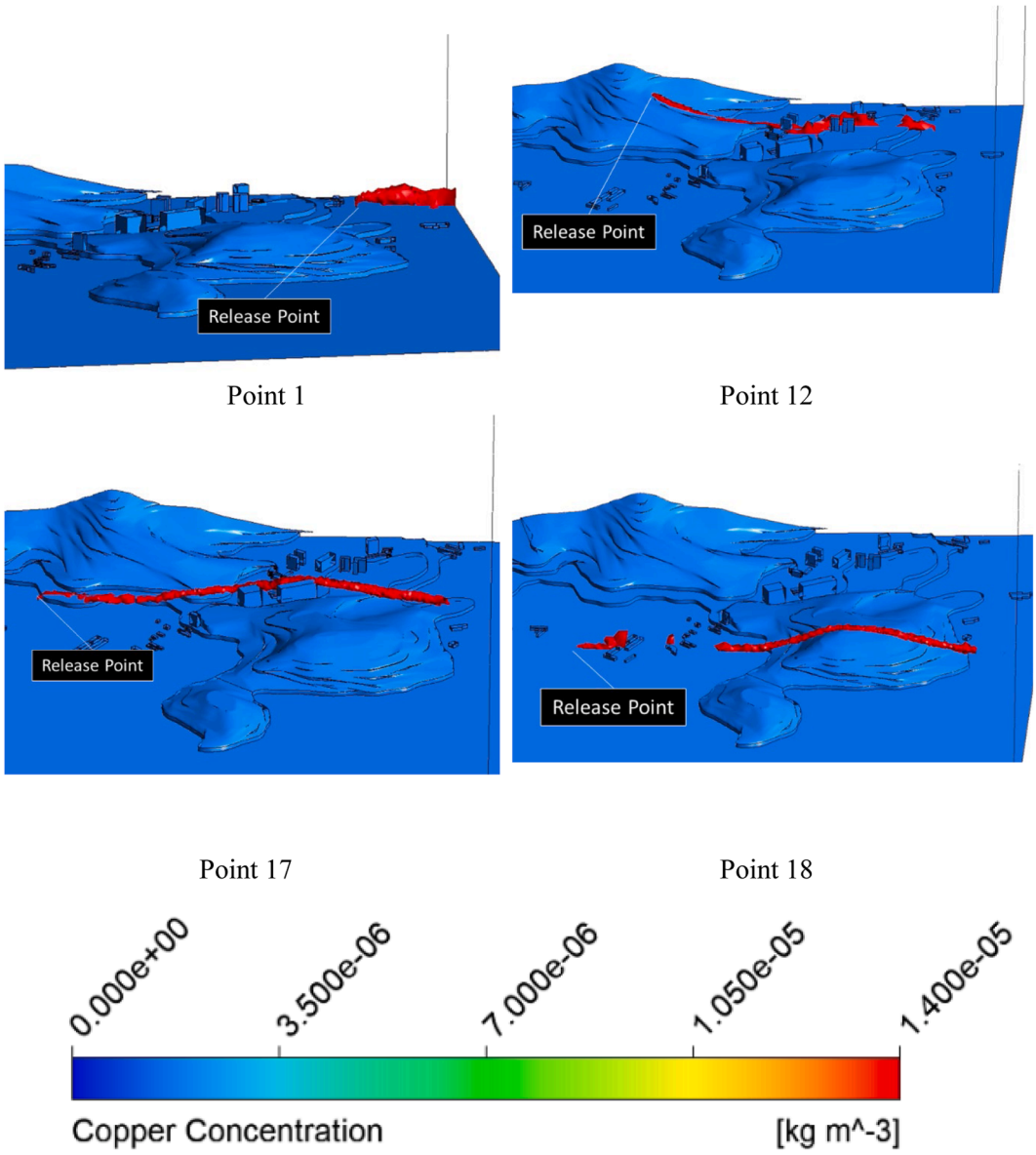

Fig. 11. Copper concentration isosurface plots at 1.4×10^{-5} kg/m^3 for cases of release points 1, 12, 17 and 18 under 3.4 m/s west-wind.

2.5. Sensor number reduction by ANN model

To achieve an efficient "sensor detection-combustion source location system", the number of sensors is further reduced through an ANN model. The JustNN software is able to provide an "Importance List" for each input, which will be an indicator to compare all sensors to determine the effectiveness of sensors in the detection. The importance list consists of the descending order of the summation of the absolute weights of the connections from input node to all the nodes in the first hidden layer. This implies that the concentration measured by the least important input nodes or sensors do not have much impact on the determination of the source location. First, CFD and MILP was used to sort out a total of 1611 sensors to 106 sensors. Then, from these 106 sensors, additional points were sorted out based on the importance list from the ANN. Based on the importance list, sensors with lower importance are deleted in order to test the performance of system without these low-importance sensors. The remaining sensors are used to establish a new ANN network, which is trained using the same 108 datasets. According to the initial importance list, the number of sensors is sorted and reduced multiple times to find a value that can maintain the same validation percentage but requires fewer sensors.

2.6. Neural network modelling

The Artificial Neural Networks (ANN) method was chosen as the approach to identify the source location in this study, using the JustNN software. JustNN is a neural network software that has been utilized in numerous previous studies. For instance, Al Barsh et al. (2021) employed JustNN to train an ANN model to accurately classify and predict the miles per gallon of current and future cars with a precision of 92.77 %. Similarly, in Alkronz et al. (2019) research, JustNN was applied to train a multilayer ANN model to predict whether mushrooms were poisonous or not, achieving an accuracy rate of 99.25 %. Furthermore, Yu et al. (2022) utilized JustNN in their study to predict the location of illegal plastic burning sites, proving the feasibility of CFD-ANN methodology for source location identification.

There are two objectives to train the ANN model in current work. First was to further optimize the sensor numbers required while second was to train an ANN model that was able to identify the e-waste burning location based on the optimized sensors number. Here, the input

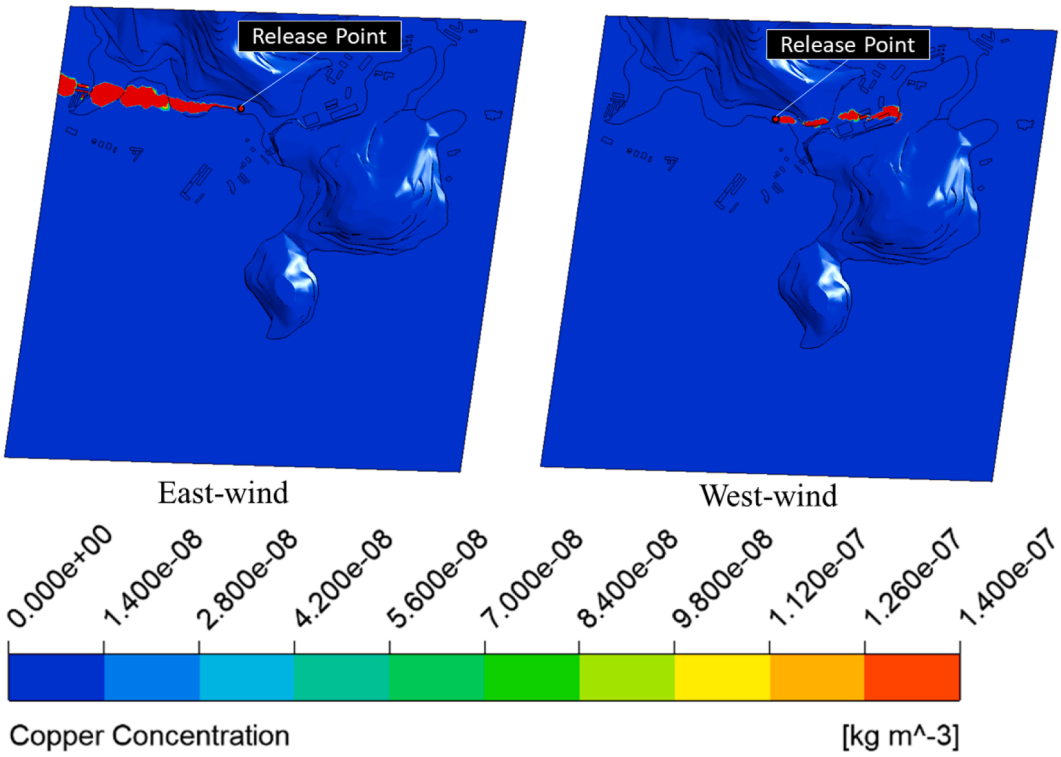

Fig. 12. Effect of wind direction at point 13 (wind speed: 5.5 m/s).

neurons are the copper concentrations at all the possible sensors while the output neurons are the 18 possible locations. For the number of hidden layers, more hidden layers may be helpful to improve the accuracy of the model, but it will greatly increase the time complexity (Uzair and Jamil, 2020). Two hidden layers are utilized for current work because the model accuracy up to 97.22 % could be achieved with the optimized number of sensor (Refer to Section 3.3 for further explanation).

The training set comprised 108 concentration datasets obtained from CFD simulation to enable the model to be trained in recognizing from the existing 18 release points. On top of the 108 training datasets, 36 validation sets, which the model had not previously learned, were utilized to evaluate the validation rate of the model. All the data was labeled using the supervised learning method to facilitate the model's learning of classification and prediction results. The model extracted the feature values and mapping relationships by learning from these labeled sample data and tried to find a function that maps the input data to the output data. The weights between neurons were adjusted accordingly by the neural network via the use of the loss function and validation rate to identify errors. During training, the loss function guides the optimization process by providing metrics for evaluating the performance of the model, i.e., adjusting the weights to minimize the value of the loss function. This process was repeated until an acceptable validation rate or error was achieved.

3. Result and discussion

3.1. CFD simulation

3.1.1. Metal concentration

Fig. 5 shows the dispersion profile for burning site 10 at east wind speed of 1.6 m/s. The inhalation reference concentration (RfC) for copper is approximately 1.4×10^{-7} kg/m^3 (Cesaro et al., 2019). Consequently, a contour plot was generated to depict copper concentrations with an upper limit of 1.4×10^{-7} kg/m^3, which can be useful for analyzing the contamination of this study area by copper particles. Because the study area has high and undulating topography, the contour plot was set at 50 m altitude to display the copper concentrations accurately across the entire region.

The dispersion profile clearly indicates that copper particle concentration was extremely high at the point of release. Subsequently, because of wind influence, the plume gradually expanded, and the impacted area became wider. Upon reaching the boundary of the study area, it was revealed that copper concentrations had decreased, with some regions exhibiting concentrations below RfC value. Nevertheless, despite the diminishing concentrations, the highest concentration at the boundary, the greatest distance from the release point, remains above the RfC value. Undoubtedly, this indicates that open burning of electronic waste can pose a serious risk of heavy metal exposure to the surrounding population.

3.1.2. Terrain effect

Given the introduction of terrain and buildings in the 3D geometry, it is of great interest to observe how copper flow is impacted by these obstacles. Obstacles affect the diffusion of copper particles in two main ways, one is the change of direction and path and the other is the tendency to generate turbulence. The complex topography of high mountains can lead to multi-directional changes in airflow, creating complex movement patterns and making the diffusion path of copper particles more variable. Localized turbulence caused by high mountains or high buildings will increase the mixing and diffusion rate of particles, making their distribution in the air more extensive and complex, and generating eddies and reflux zones on the leeward side, which will increase the concentration of particles some localized spots. It was found that due to the presence of obstacles such as terrain and buildings, copper particle streams are subjected to different drag and lift forces as well as pressure variations, and therefore their direction of diffusion is more affected.

The use of iso-surfaces for copper concentrations at 1.4×10^{-7} kg/m^3, with reference to the maximum RfC value was applied in investigating the effects of flow in the study area, as depicted in Fig. 6. The copper concentrations within the region of the iso-surface were higher than the RfC value. In short, the copper concentrations in the

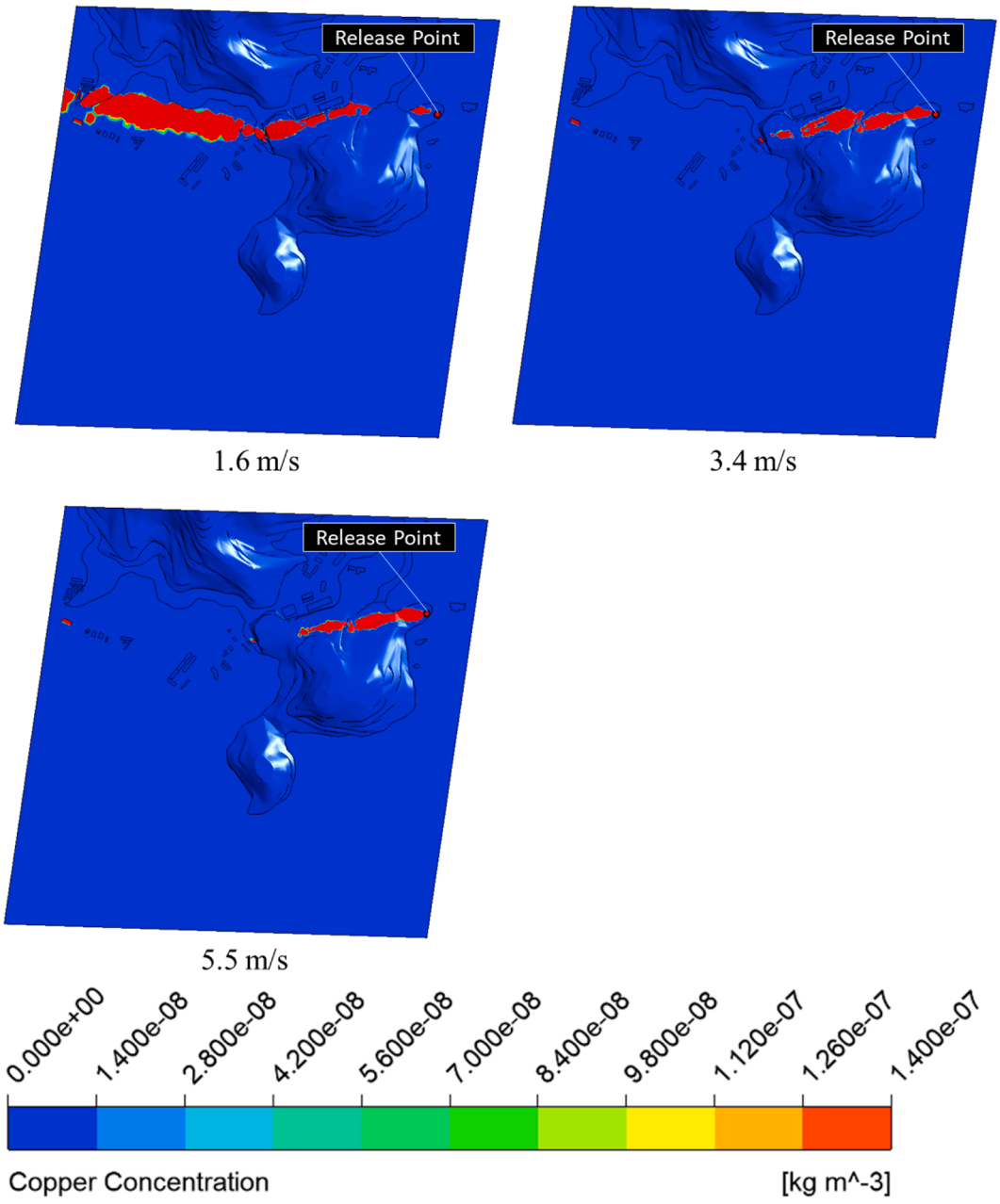

Fig. 13. Effect of wind speed at point 2 under east-wind.

region shown in the figure that in touch with the iso-surface was higher than RfC value, which was unsafe.

The case of point 1 under 3.4 m/s east-wind (Case 2) reveals that when fluid encounters high mountain barriers, it moves up the mountain, and gradually affects the lower terrain as it spreads out. The presence of obstacles can contribute to the deflection of the plume and subsequent movement of the plume upward over the obstacles, allowing the plume to be dispersed to greater heights compared to unobstructed cases (Galeev et al., 2013a). Upon encountering a gap between two mountains, as observed in the case of east-wind at point 5 (Case 26), the flow was obstructed and followed the mountain instead of the direction of the wind. The trajectory of the copper particle flow in Case 26 also became further confined by two towering buildings on its right and the hill below. Unlike in Case 1, the plume in Case 26 did not rise nor split when encountering the obstacles. This could be due to the combined hinderance effect provided by the two buildings and the mountains, which flanked the plume, creating a canyon-type geometry which controlled and directed the flow of the plume. Only after leaving the canyon, the direction of the plume was then directed by the wind. Upon leaving the mountainous areas and taller buildings, the fluid flow gradually spread out in open areas as no obstacles were close or large enough to block and affect the dispersion.

For burning at point 14 under west wind (Case 80), unlike Case 2, the fluid sinked directly after flowing over the hill, thus contaminating the ground; this is possibly due to the hill being lower in Case 80 with a height of up to 150 m, in contrast to the larger hill in the north at a height of about 200 m. The size and height of obstacles can significantly impact plume dispersion as observed by Xu et al. (2023) and Derudi et al. (2014) where in the case of a lower obstacle, the plume can easily cross over and gather behind the obstacle, creating high concentration zones in front and behind the obstacle, similar to that as seen in Case 80. When the obstacle is sufficiently tall, the plume may be blocked entirely or the plume may also cross over but move higher and is blown away by the wind, rather than fall back down behind the obstacle, as observed in

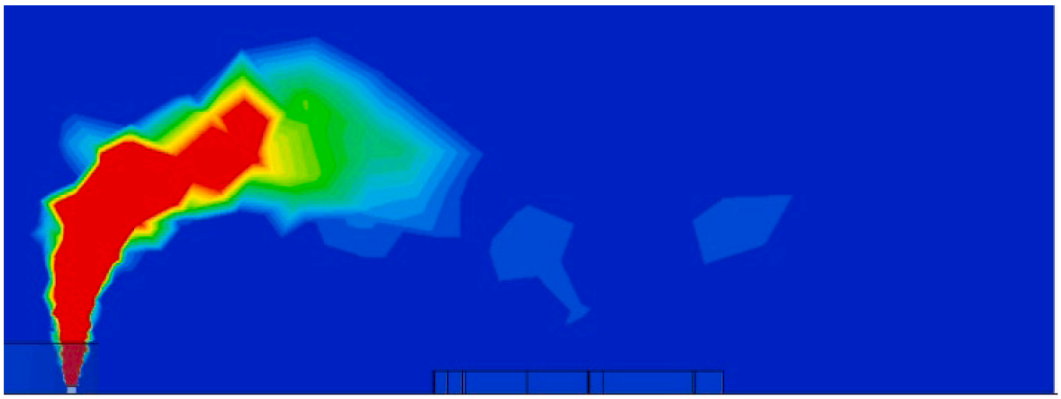

1.6 m/s

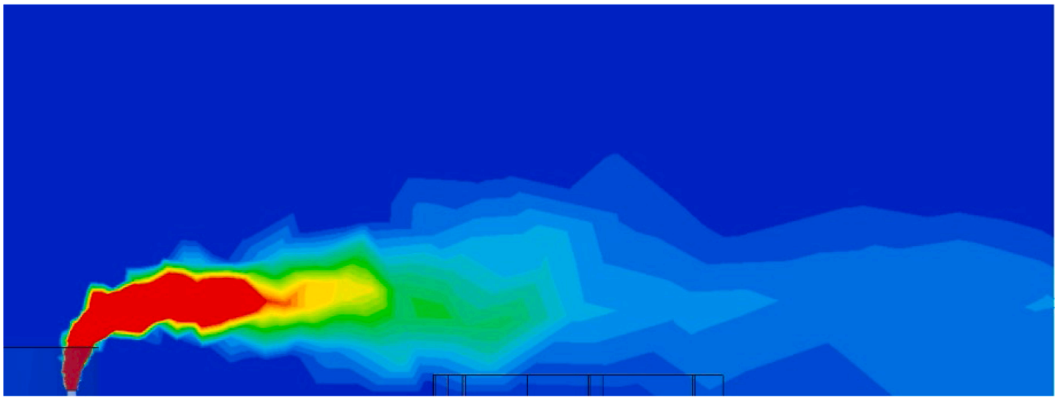

3.4 m/s

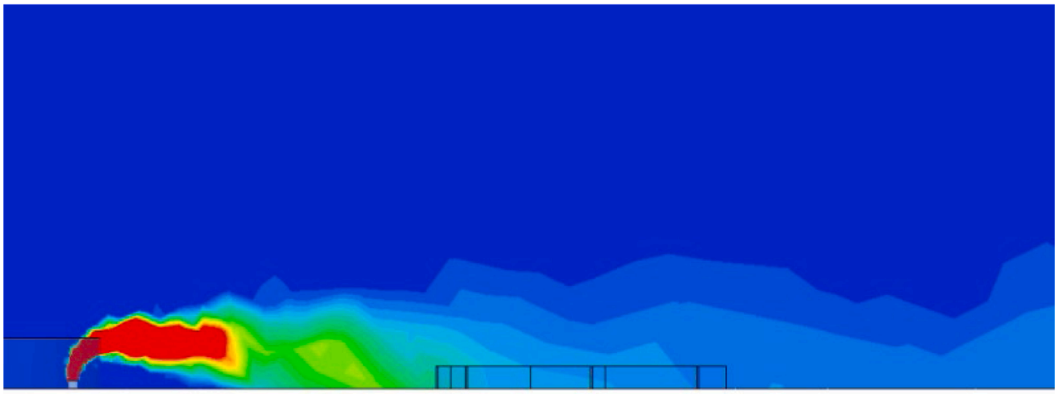

5.5 m/s

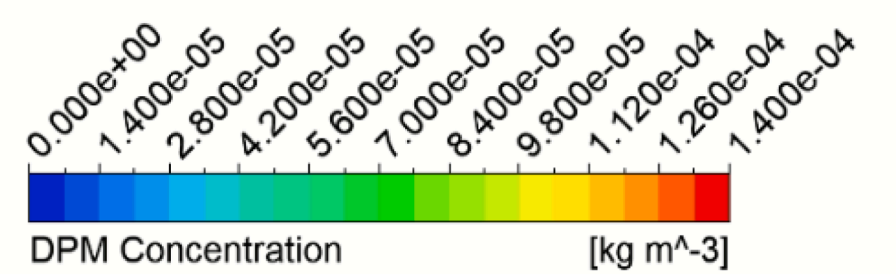

Fig. 14. Side view of three cases release from point 1 under west-winds.

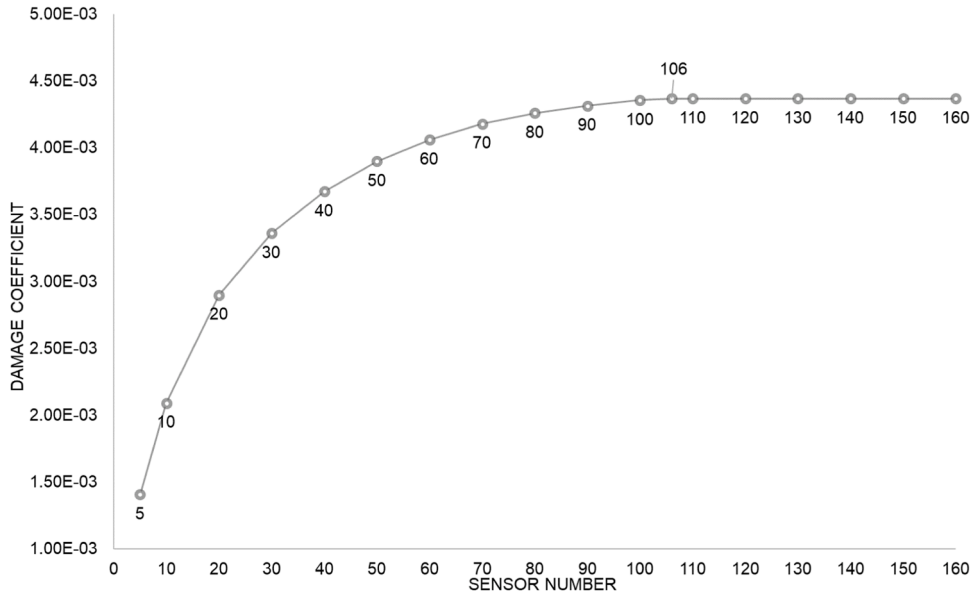

Fig. 15. Relationship between sensor number and damage coefficient.

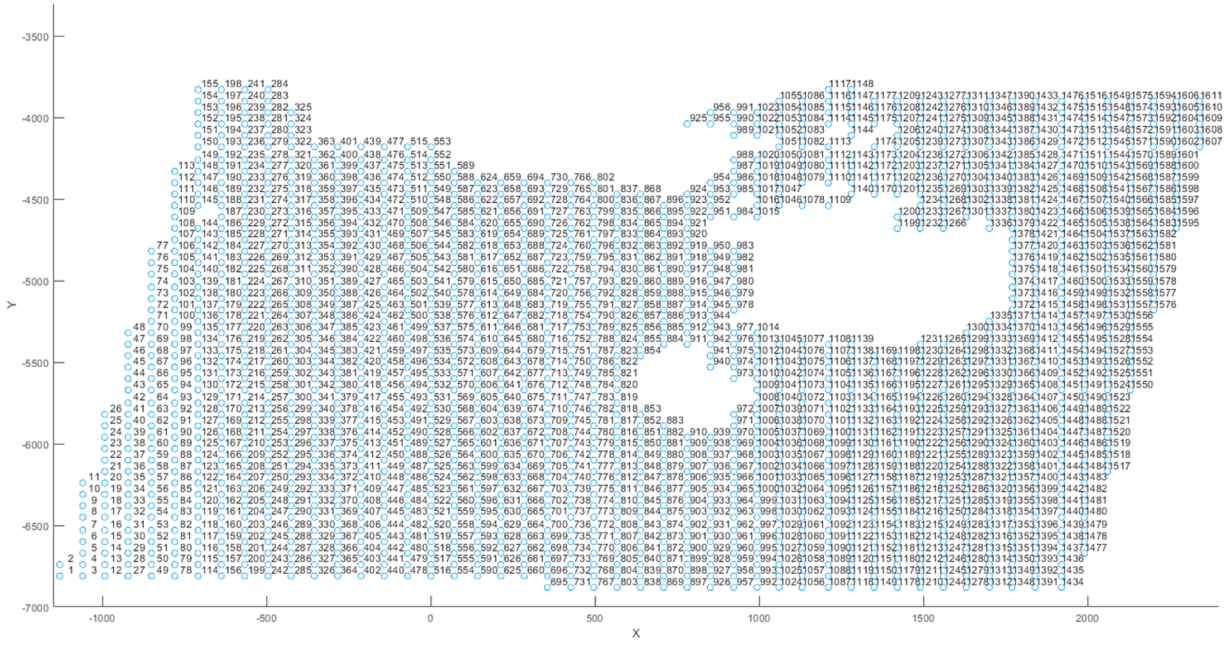

Fig. 16. Initial 1611 sensor candidates' locations.

Case 1.

At point 17 and west wind (Case 101), since the release point is on the west side and the wind blows from the west to east, the copper particle flow is blocked first by the mountain upon entering the middle area and subsequently influenced by buildings. The flow passes from the north of the building before gradually spreading out and affecting the surrounding residential areas. Initially, the plume blew towards the west due to the west wind and was slightly redirected as it moved between the two mountains in the canyon or valley zone. After the valley, the plume returned to moving towards the western direction for some short distance before encountering obstacles in the form of buildings, which was similar in height to the 150 m mountain in Case 80. This caused the plume in Case 101 to cross and subsequent fall over the building in the same manner as when the plume in Case 80 encountered the mountain (Derudi et al., 2014; Xu et al., 2023).

The impact of terrain effects is more obvious when using higher concentration isosurfaces of 1.4×10^{-5} kg/m^3, as shown in Fig. 7. The higher concentration copper fluid in Case 2 under 3.4 m/s east-wind with point 1 that was obstructed by the high mountain managed maintain the higher concentration even after rising along the mountain terrain and moving at the higher heights. In Case 80 at point 18 and Case 101 at point 17, both with 3.4 m/s west-wind, the higher concentration isosurface fluid plot also maintained the concentrated flows across the shorter mountain and building obstacles, respectively. However, the higher concentration isosurfaces clearly indicated some degree of drop of the plume in Case 80 and Case 101 after encountering their respective obstacles.

For Case 26 with point 5 under 3.4 m/s east-wind, the flow of the higher concentration fluid broke up and dispersed after leaving the mountainous areas and taller buildings into open area, as observed by

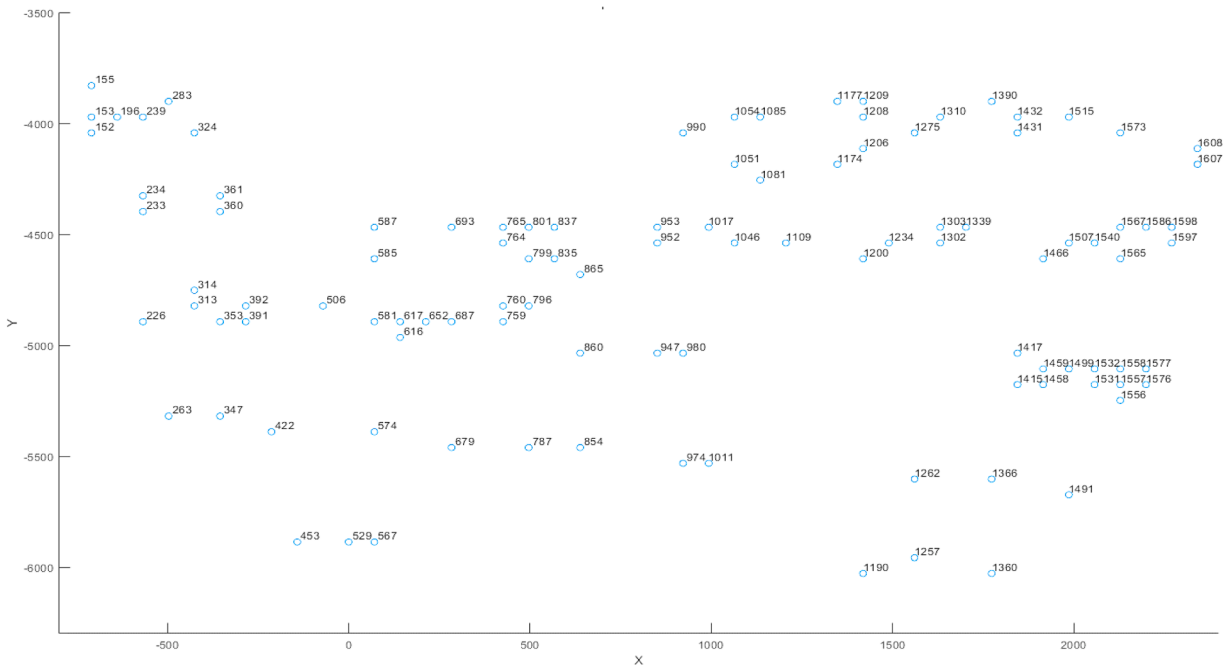

Fig. 17. The optimized 106 sensors' locations.

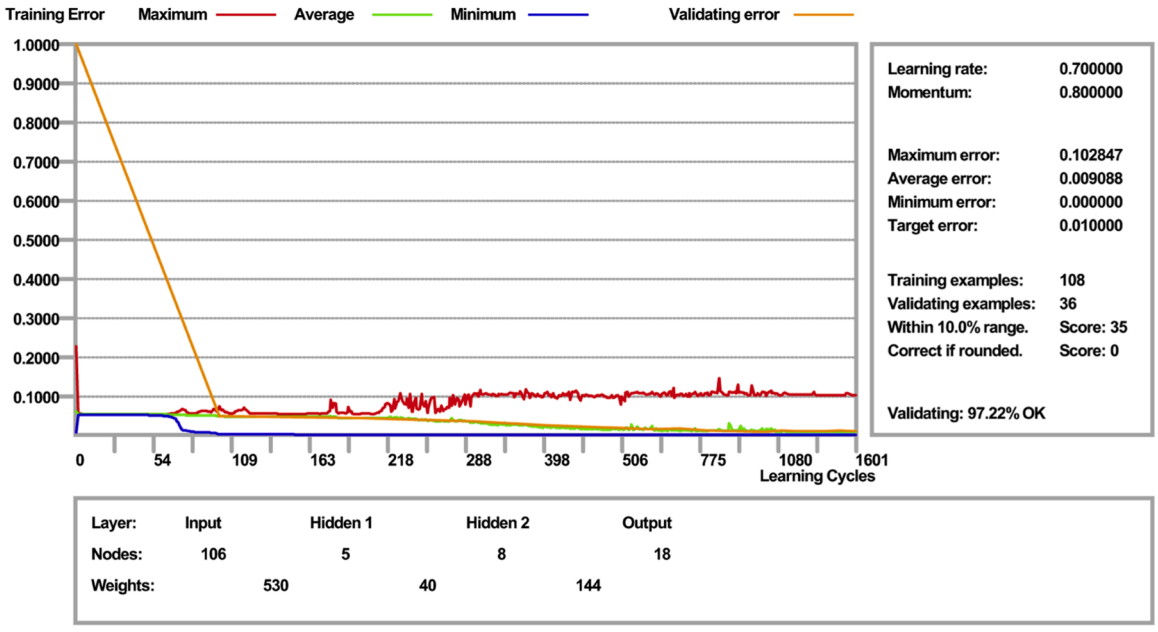

Fig. 18. Result graph of the ANN model.

the gradual disappearance of the higher concentration isosurface plots. For Case 26, the copper particle fluid concentration contours (Fig. 8) indicated the dilution of the plume after changing direction and moving into the open area, with fluid expanding from narrow and more concentrated to a wider, less concentrated plume. On the other hand, the copper particle fluid in Case 101 mostly maintained its concentration even after changing location due to the presence of obstacles, which may have impeded the dispersion. After leaving the mountainous area, the plumes in Case 2, 26, 80, and 101 all gradually lowered in concentration. Due to the absence of obstacles, the plume further away from the source readily mixed and was diluted with the surrounding air. The combination of buildings and terrain has complex effects on the dispersion and diffusion of the fluid as well as the shape and size of the concentrated fluid plumes.

From the concentration contour figures (Fig. 8), the copper particle fluids in Case 2 and Case 80 can be observed to travel far whilst maintaining their concentration and only dispersed after passing their respective mountainous areas. It can also be observed that there is some dilution of the plume after encountering the areas populated with buildings for Case 2 and Case 80. The presence of the buildings caused portion of the plume to be deflected and split up to move along the sides of the buildings, leading to decreased pollutant concentration in the centreline downwind from the release as well as the leeward side of the obstacles (Galeev et al., 2013b). There is also accumulation of larger, high concentration zones in the windward side of the obstacles, as noted in plume concentration isosurfaces in Fig. 6 and concentration contours

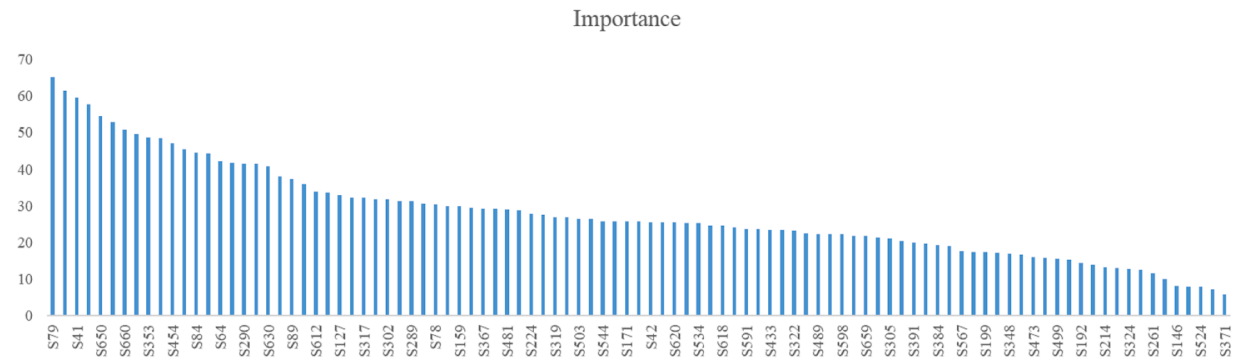

Fig. 19. Importance list for the first 100 sensors obtained from the original 106-sensor ANN model.

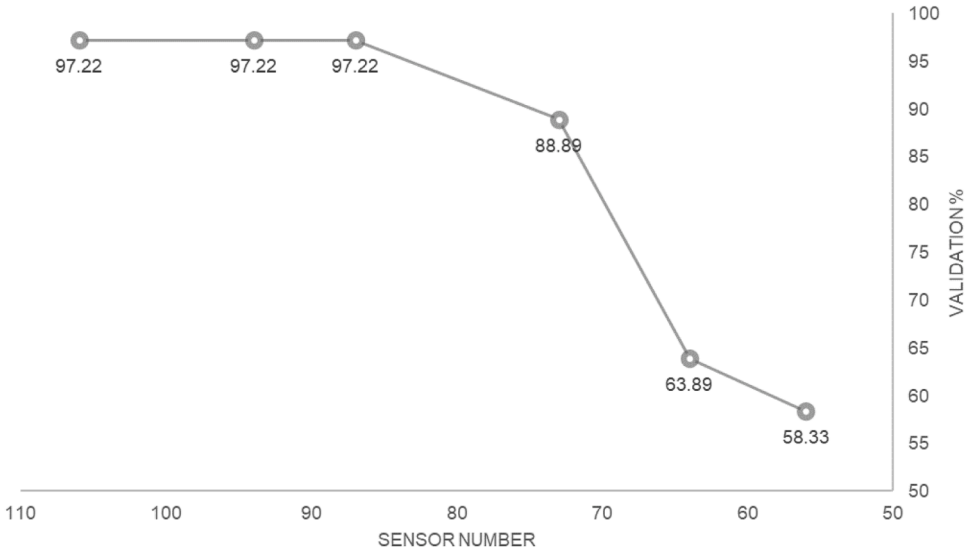

Fig. 20. Validation percentage of ANN models with different sensor numbers.

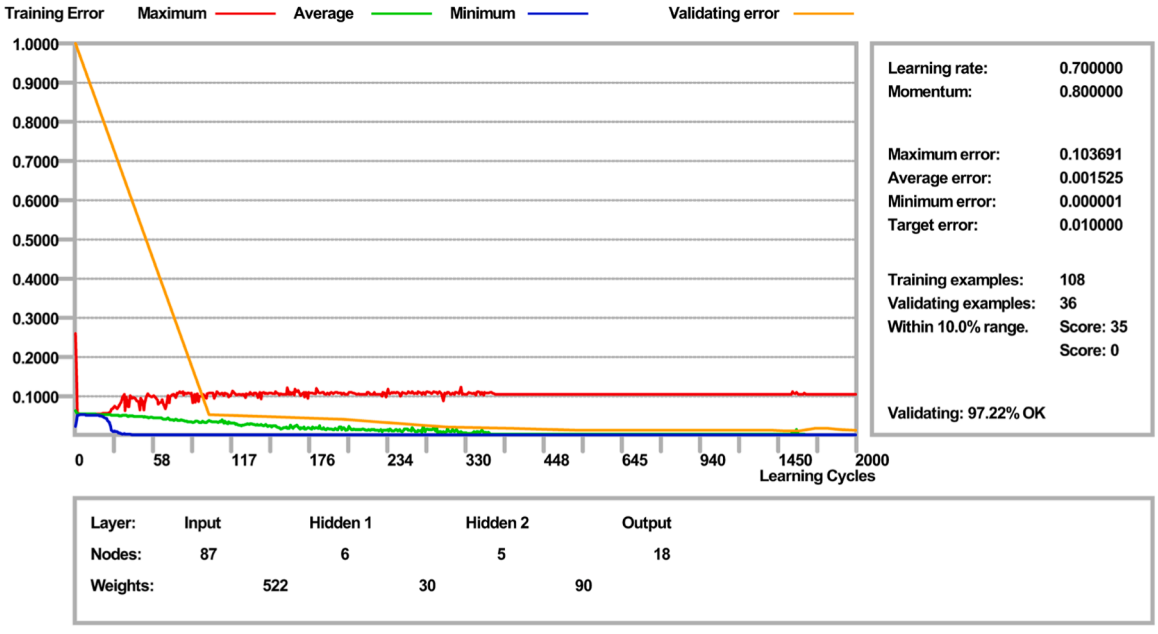

Fig. 21. Result graph of 87-sensors ANN model.

Fig. 22. The final 87 sensors locations.

in Fig. 8 for Case 2 and Case 101. Moreover, the concentration contours also showcased the dispersion of the plume where it was observed that the plume in Case 2 did not fall down after crossing over the higher 200 m mountain. While in Case 80 and Case 101, the concentration contours clearly illustrated the falling of the plume after the 150 m tall mountain and the tall building, respectively.

3.1.3. *Burning location effect*

As the dispersion distribution and contaminated areas may vary significantly based on different release sites, four representative sites with fixed wind direction and speed were selected for analysis, as shown in Fig. 9. Point 1, in close proximity to the eastern boundary, was observed to have a limited affected area under a west wind. This has reached the limits of scope in this study. Combined with the map, it can be seen that outside the eastern boundary is the Penang International Airport, with no obstacles in the form of buildings or terrain. Therefore, based on the results from other release sites, it is reasonable to assume that the area to the east of this release site may be heavily contaminated, though the lack of obstacles may possibly cause minimal vertical and horizontal diffusion of the highly concentrated copper particle fluid until some distance away from the source. Conversely, at point 12, located on the eastern side of the mountain where there are a few obstacles to impact dispersion under a west wind, the contaminated area was larger. From the concentration contours in Fig. 10, it can be observed that there is significant vertical and horizontal diffusion whenever the copper particle fluid encountered obstacles, increasing the size of the contaminated area and showcasing the blocking effect of obstacles against gas dispersion. In contrast, point 17 encountered a middle area with two mountains and many tall buildings, resulting in greater obstruction, and thus, a smaller area with higher copper particle concentration than point 12.

The blocking effect was weaker here with release point 17 as the obstacles were not directly along the path of the copper particle dispersion, as illustrated in the isosurface plots in Fig. 11. For point 18, although the residential area on the west end of the mountain was heavily contaminated, the dispersion of copper particles in the area situated on the east end of the mountain was blocked by the mountain, resulting in no significant contamination. As the copper particles passed along the mountain, the fluid was highly concentrated without significant vertical and horizontal diffusion until travelling some distance by leaving the mountainous area into a more open location. Moreover, each release point would affect a distinct residential area; for example, the northeast corner was contaminated in the case of point 12, but it would remain unaffected in the case of point 18.

3.1.4. *Effect of wind direction*

Fig. 12 compares the effect of wind direction on the dispersion profile of copper particles at point 13 with a wind speed of 5.5 m/s. The comparison clearly illustrates the crucial role played by wind direction in the dispersion range of copper particle flow. If the wind is from the west, the eastern side of the release point is more contaminated, and vice versa. It can be concluded that establishing an effective monitoring system to detect copper concentration across the entire area is challenging, indicating the need for subsequent optimization of sensor placement.

The effect of wind direction on the dispersion profile is compared in the. Here the two wind directions are compared at point 13 at a wind speed of 5.5m/s. The wind direction plays a crucial role in the dispersion range of the copper particle flow. If the wind is from the west, the eastern side of the release point will be more contaminated, and vice versa. This means that it is difficult to establish an effective monitoring system to detect the copper concentration covering the whole area, indicating that the subsequent optimization of the sensor placement is necessary.

3.1.5. Effect of wind speed

Furthermore, wind speed is a key factor in the dispersion of copper particle flow. Fig. 13 presents three profiles at point 2, with three varying wind speeds (1.6, 3.4, and 5.5 m/s), all in the same wind direction (east wind). It is evident that at slower wind speeds, a larger area is affected by copper particles despite having the same release point and wind direction. In the case of 1.6 m/s wind speed, the affected area was continuous from the release point until the boundary of the study area. However, when wind speed was 5.5 m/s, after passing over the hill, the copper particles did not affect the residential area near to the west of the hill but affected a small area at about 2.5 km downwind. The area that was affected by copper particles is found to be reducing with higher wind speed, as shown in Fig. 14, which contained side-view figures of the gas dispersion from point 1 under the three wind speeds. The copper particles in the air were dispersed and blown further away from the release point at higher wind speed. Thus, the copper concentration was reduced with the higher wind speed, which is the same concept as the Pasquill-Gifford dispersion model.

3.2. Sensor optimization

To train an accurate machine learning model for ignition point identification, effective concentration data must be provided to the algorithm. The MILP method was used to optimize sensor placement and minimize the number of sensors needed while still providing sufficient concentration data. The optimal sensor locations were selected to obtain the required concentration data.

The LINGO 20.0 software was utilized to optimize the sensor arrangement using the MILP method. Sensor numbers were tested from 5 to 160 in order to determine the optimal value that would maximize the damage coefficient. The software was able to calculate the optimal result for one test within a few minutes. The outcome of this optimization process is displayed in Fig. 15.

The damage factor exhibits significant growth as the number of sensors increases from 5 to 50. When the number of sensors reaches 100, the curve becomes entirely smooth, and the damage factor nearly approaches its maximum level. Consequently, after reaching 100 sensors, the change in the damage coefficient for each additional sensor was tested. The optimal value, identified as the minimum number of sensors required to maximize the damage factor, was found to be 106 sensors.

The locations of sensors are illustrated in Fig. 16. Initially, sensor candidates were generated uniformly on the 50 m height plane, resulting in 1611 sensor candidates. Following optimization, the number of sensors drastically decreased to 106, yet they still cover a significant portion of the area.

Although the optimized sensor placement successfully maximizes the damage coefficient, it is worth noting that some sensors are in close proximity to one another, such as the 12 sensors on the right side (including 1531, 1532, 1557, 1558, etc.). While these closely situated sensors may contribute to the maximization of the damage coefficient, the actual detection may experience overlapping issues. The proximity of sensors creating overlapping detection areas can be an indication of the areas having a larger overlap of pollutant dispersion and hence require additional number of sensors to detect and measure the pollutant concentration in these areas in order to more accurately ascertain the damage coefficient. The occurrence of overlapping sensor detection areas or some sensors in close proximity can also be seen in gas detector placement optimization studies (Benavides-Serrano et al., 2013; Lee et al., 2024; Liu et al., 2020; Sun et al., 2020). Hence, further optimization of sensor placement may be necessary to ensure the practicality of the current results.

3.3. ANN model for source tracking

The ANN model was built for source localization of e-waste burning sites and was used to further optimize the number of sensors after successfully verifying the feasibility and accuracy of source localization. To identify and track the e-waste open burning sites, the ANN model was generated by the concentration data from the MILP optimized 106 sensors, as shown in Fig. 17. The network comprises of an input layer with 106 neurons, a first hidden layer consisting of 5 neurons, a second hidden layer consisting of 8 neurons, and an output layer with 18 neurons. During the training phase, the neural network identifies patterns using 108 sets of CFD data. The concentration data from the 106 sensors is inputted into the 106 input neurons. Additionally, release point data is provided to the 18 output neurons. The learning rate and momentum rate were optimized by the JustNN software and fixed at 0.7 and 0.8 respectively. Validation was conducted each 100 cycles and 10 % error of desired outputs were accepted. The learning process was stopped only when 95 % of the examples were validated within the accepted error. The weights between neurons were adjusted accordingly by the ANN via the use of the loss function and validation rate to identify errors. The scaled input, activation parameters, bias, and error of each node can be obtained from the JustNN software.

The result is shown in Fig. 18. After 1601 cycles, the model achieved 97.22 % validation percentage indicating the neural network was able to effectively match the concentration profiles and the release points during the training. Out of the 36 validation sets, the trained ANN model successfully assessed 35 sets of e-waste burning locations. The average error rate of this model is approximately 0.9088 %, which is below the target of 1 %. These findings demonstrate the feasibility of the ANN model and its exceptional ability to detect open burning sites in large, multi-obstacle environments with only the concentration information from 106 sensors.

From the importance list shown in Fig. 19 sensor 79 has the highest importance, 65.1761. More than half of the 100 sensors listed had an importance index below 25. Consequently, five new ANN models were constructed based on the importance ranking. The models had minimum importance limits of 10, 15, 20, 23, and 25, respectively.

Fig. 20 demonstrates that the validation percentage of the ANN model remains steady at 97.22 % when the number of sensors is reduced to 94 and 87. However, when the number of sensors is further reduced to 84, the validation percentage gradually decreases and drops to 88.89 %. Additionally, when the number of sensors was reduced to 64 and 56, the validation percentage plummeted to 63.89 % and 58.33 %, respectively. Based on these results, it can be concluded that the optimal number of sensors for this experiment is 87, which maintains the verification percentage at 97.22 %.

In the 87-sensor model, the training error was only 0.1525 % after 2000 cycles, as shown in Fig. 21. The locations of the 87 sensors are plotted in Fig. 22, and a comparison with the original 106-sensor locations indicates that some sensors with overlapping ranges have been removed, such as sensor No.391, No.1417, and No.1558. The remaining 87 sensors, as sensors of high importance, can continue to provide a good validation rate to detect the location of the release point. This means that the number of sensors can be reduced to minimize costs and to preserve good detection efficiency.

The ANN model built with JustNN in this study is capable of accurately identifying the location of illegal e-waste open burning sites. This model relies on reliable CFD simulation data to efficiently pinpoint the burn sites. By utilizing data from 106 sensors, the trained model can determine the release point location without requiring additional wind speed and direction information, resulting in an effective and efficient system. Moreover, reducing the number of sensors demonstrated that 87 sensors are adequate to achieve the same function with a 97.22 % validation accuracy. This model provides a fast and reliable method for identifying the location of e-waste burning. By using these 87 sensors and the ANN model, e-waste burning sites can be identified immediately once an abnormal concentration of copper particles is detected, allowing for early detection and control of illegal e-waste burning. This is crucial for protecting the urban environment and residents from toxic substances.

4. Conclusion

This study presents a novel CFD-MILP-ANN method for identifying the source location of open burning of e-waste with sensor placement and number optimization. The dispersion profile of copper particle releases was simulated by CFD for a 3 km x 3 km area on Penang Island, Malaysia. Subsequently, the concentration profiles obtained were employed to optimize the sensor arrangement for the MILP method. The optimization yielded a reduction of the total number of sensors required for the detection of burning operations to 106. An ANN model was trained using concentration data from 106 sensors. The model consists of 106 input neurons, 13 hidden neurons laid out in two layers (5 for layer 1 and 8 for layer 2), and 18 output neurons. The trained ANN model achieved a validation percentage of 97.22 % for 36 unlearned validation sets. By further reducing the sensors based on the ANN model, it was found that only 87 sensors were needed to achieve the same 97.22 % validation for open-air combustion source identification. This indicates that the source localization by ANN model can be used to quickly identify and precisely locate the e-waste burning activities in the region. In conclusion, the combination of CFD simulation, MILP optimization, and the ANN model provides a highly precise and efficient method for toxic gas source localizations. This simple and fast method exhibits great potential for early prevention and protection of residents from hazardous substances while embracing Sustainable Development Goal target 3.9.

CRediT authorship contribution statement

Yiming Lang: Writing – original draft, Validation, Formal analysis, Data curation. **Michelle Xin Yi Ng:** Investigation. **Kai Xiang Yu:** Writing – review & editing. **Binghui Chen:** Resources. **Peng Chee Tan:** Supervision. **Khang Wei Tan:** Writing – review & editing. **Weng Hoong Lam:** Methodology. **Parthiban Siwayanan:** Conceptualization. **Kek Seong Kim:** Writing – review & editing. **Thomas Shean Yaw Choong:** Writing – review & editing, Methodology. **Joon Yoon Ten:** Methodology. **Zhen Hong Ban:** Supervision.

Declaration of competing interest

The authors declare that they have no known competing financial interests or personal relationships that could have appeared to influence the work reported in this paper.

Acknowledgements

The authors would like to acknowledge the financial support provided by the Xiamen University Malaysia Research fund (Grant number: XMUMRF/2018-C1/IENG/0002) and Xiamen University Malaysia External Research Fund supported by Hengyuan International Sdn. Bhd. (Grant Number: EENG/0003).

References

Achtemeier, G.L., Goodrick, S.A., Liu, Y., Garcia-Menendez, F., Hu, Y., Odman, M.T., 2011. Modeling smoke plume-rise and dispersion from Southern United States prescribed burns with Daysmoke. Atmosphere 2 (3), 358–388. https://doi.org/10.3390/atmos2030358.

Al Barsh, Y.I., Duhair, M.K., & Ismail, H.J. (2021). MPG prediction using just NN. http://dspace.alazhar.edu.ps/xmlui/handle/123456789/2711.

Alkronz, E.S., Moghayer, K.A., Meimeh, M., Gazzaz, M., Abu-Nasser, B.S., & Abu-Naser, S.S. (2019). Prediction of whether mushroom is edible or poisonous using back-propagation neural network. http://dspace.alazhar.edu.ps/xmlui/handle/123456789/126.

Allen, C., Young, G., Haupt, S., 2007. Improving pollutant source characterization by better estimating wind direction with a genetic algorithm. Atmos. Environ. 41 (11), 2283–2289. https://doi.org/10.1016/j.atmosenv.2006.11.007.

Annunzio, A.J., Young, G.S., Haupt, S.E., 2012. Utilizing state estimation to determine the source location for a contaminant. Atmos. Environ. 46, 580–589. https://doi.org/10.1016/j.atmosenv.2011.04.080.

ANSYS. (2020). *ANSYS fluent theory guide.*

Baalisampang, T., Saliba, E., Salehi, F., Garaniya, V., Chen, L., 2021. Optimisation of smoke extraction system in fire scenarios using CFD modelling. Process Saf. Environ. Protect. 149, 508–517. https://doi.org/10.1016/j.psep.2020.11.036.

Benavides-Serrano, A.J., Legg, S.W., Vázquez-Román, R., Mannan, M.S., Laird, C.D., 2013. A stochastic programming approach for the optimal placement of gas detectors: unavailability and voting strategies. Ind. Eng. Chem. Res. 53 (13), 5355–5365. https://doi.org/10.1021/ie401369v.

Benavides-Serrano, A.J., Mannan, M.S., Laird, C.D., 2015. A quantitative assessment on the placement practices of gas detectors in the process industries. J. Loss. Prev. Process. Ind. 35, 339–351. https://doi.org/10.1016/j.jlp.2014.09.010.

Bernama, 2022. Container with E-waste to be Returned to United States — Penang DOE, 2022/12/08. The Edge Markets.

Boikos, C., Siamidis, P., Oppo, S., Armengaud, A., Tsegas, G., Mellqvist, J., Conde, V., Ntziachristos, L., 2024. Validating CFD modelling of ship plume dispersion in an urban environment with pollutant concentration measurements. Atmos. Environ. 319, 120261. https://doi.org/10.1016/j.atmosenv.2023.120261.

Cantelli, A., D'Orta, F., Cattini, A., Sebastianelli, F., Cedola, L., 2015. Application of genetic algorithm for the simultaneous identification of atmospheric pollution sources. Atmos. Environ. 115, 36–46. https://doi.org/10.1016/j.atmosenv.2015.05.030.

Cen, K., Yao, T., Wang, Q., Xiong, S., 2018. A risk-based methodology for the optimal placement of hazardous gas detectors. Chin. J. Chem. Eng. 26 (5), 1078–1086. https://doi.org/10.1016/j.cjche.2017.10.031.

Cesaro, A., Belgiorno, V., Gorrasi, G., Viscusi, G., Vaccari, M., Vinti, G., Jandric, A., Dias, M.I., Hursthouse, A., Salhofer, S., 2019. A relative risk assessment of the open burning of WEEE. Environ. Sci. Pollut. Res. Int. 26 (11), 11042–11052. https://doi.org/10.1007/s11356-019-04282-3.

Chaubey, J., Srivastava, R., 2020. Simultaneous identification of groundwater pollution source location and release concentration using Artificial Neural Network. Environ. Forens. 23 (3–4), 293–300. https://doi.org/10.1080/15275922.2020.1850566.

Chen, S., Du, W., Peng, X., Cao, C., Wang, X., Wang, B., 2022. Peripheric sensors-based leaking source tracking in a chemical industrial park with complex obstacles. J. Loss. Prev. Process. Ind. 78, 104828. https://doi.org/10.1016/j.jlp.2022.104828.

Cho, J., Kim, H., Gebreselassie, A.L., Shin, D., 2018. Deep neural network and random forest classifier for source tracking of chemical leaks using fence monitoring data. J. Loss. Prev. Process. Ind. 56, 548–558. https://doi.org/10.1016/j.jlp.2018.01.011.

Chow, F.K., Kosovic, B., & Chan, S.T. (2005, 2005-11-04). Source Inversion for contaminant plume dispersion in urban environments using building-resolving simulations. United States.

Davis, J.M., Garb, Y., 2019. A strong spatial association between e-waste burn sites and childhood lymphoma in the West Bank, Palestine. Int. J. Cancer 144 (3), 470–475. https://doi.org/10.1002/ijc.31902.

Derudi, M., Bovolenta, D., Busini, V., Rota, R., 2014. Heavy gas dispersion in presence of large obstacles: selection of modeling tools. Ind. Eng. Chem. Res. 53 (22), 9303–9310. https://doi.org/10.1021/ie4034895.

Du, Y., Blocken, B., Abbasi, S., Pirker, S., 2021. Efficient and high-resolution simulation of pollutant dispersion in complex urban environments by island-based recurrence CFD. Environ. Model. Softw. 145, 105172. https://doi.org/10.1016/j.envsoft.2021.105172.

Fernández-Pacheco, V.M., Fernández-Tena, A., Ackermann, T., Blanco-Marigorta, E., Álvarez-Álvarez, E., 2023. Physical and CFD model used in the analysis of particles dispersion. Heliyon 9 (11). https://doi.org/10.1016/j.heliyon.2023.e21330.

Fontanini, A.D., Vaidya, U., Ganapathysubramanian, B., 2016. A methodology for optimal placement of sensors in enclosed environments: a dynamical systems approach. Build. Environ. 100, 145–161. https://doi.org/10.1016/j.buildenv.2016.02.003.

Forti, V., Baldé, C.P., Kuehr, R., & Bel, G. (2020). The Global E-waste Monitor 2020. 120.

Galeev, A.D., Salin, A.A., Ponikarov, S.I., 2013a. Consequence analysis of aqueous ammonia spill using computational fluid dynamics. J. Loss. Prev. Process. Ind. 26 (4), 628–638. https://doi.org/10.1016/j.jlp.2012.12.006.

Galeev, A.D., Starovoytova, E.V., Ponikarov, S.I., 2013b. Numerical simulation of the consequences of liquefied ammonia instantaneous release using FLUENT software. Process Saf. Environ. Protect. 91 (3), 191–201. https://doi.org/10.1016/j.psep.2012.05.002.

Gangwar, C., Choudhari, R., Chauhan, A., Kumar, A., Singh, A., Tripathi, A., 2019. Assessment of air pollution caused by illegal e-waste burning to evaluate the human health risk. Environ. Int. 125, 191–199. https://doi.org/10.1016/j.envint.2018.11.051.

Gökelma, M., Birich, A., Stopic, S., Friedrich, B., 2016. A review on alternative gold recovery re-agents to cyanide. J. Mater. Sci. Chem. Eng. 04 (08), 8–17. https://doi.org/10.4236/msce.2016.48002.

Hassan, E.I., Shirazi, N.S., 2021. Electronic and electrical waste management: Malaysia and Sweden experiences. In: Ali, S.N., Jumat, Z.H., Ali, S.N., Jumat, Z.H. (Eds.), Islamic Finance and Circular Economy: Connecting Impact and Value Creation, pp. 321–335. https://doi.org/10.1007/978-981-16-6061-0_16.

Haupt, S.E., Allen, C.T., Young, G.S., 2006. A genetic algorithm method for sensor data assimilation and source characterization. In: The 2006 IEEE International Joint Conference on Neural Network Proceedings.

Haupt, S.E., Young, G.S., Allen, C.T., 2007. A genetic algorithm method to assimilate sensor data for a toxic contaminant release. J. Comput. 2 (6). https://doi.org/10.4304/jcp.2.6.85-93.

Holmes, N.S., Morawska, L., 2006. A review of dispersion modelling and its application to the dispersion of particles: an overview of different dispersion models available. Atmos. Environ. 40 (30), 5902–5928. https://doi.org/10.1016/j.atmosenv.2006.06.003.

Huang, C.L., Bao, L.J., Luo, P., Wang, Z.Y., Li, S.M., Zeng, E.Y., 2016. Potential health risk for residents around a typical e-waste recycling zone via inhalation of size-fractionated particle-bound heavy metals. J. Hazard. Mater. 317, 449–456. https://doi.org/10.1016/j.jhazmat.2016.05.081.

Ioannidis, G., Li, C., Tremper, P., Riedel, T., Ntziachristos, L., 2024. Application of CFD modelling for pollutant dispersion at an urban traffic hotspot. Atmosphere 15 (1), 113. https://www.mdpi.com/2073-4433/15/1/113.

Karatas, M., 2020. A multi-objective bi-level location problem for heterogeneous sensor networks with hub-spoke topology. Comput. Netw. 181, 107551. https://doi.org/10.1016/j.comnet.2020.107551.

Keats, A., Lien, F.-S., & Yee, E. (2006). *Source determination in built-up environments through Bayesian inference with validation using the MUST array and joint urban 2003 tracer experiments*.

Keats, A., Yee, E., Lien, F.-S., 2007. Bayesian inference for source determination with applications to a complex urban environment. Atmos. Environ. 41 (3), 465–479. https://doi.org/10.1016/j.atmosenv.2006.08.044.

Kim, H., Park, M., Kim, C.W., Shin, D., 2019. Source localization for hazardous material release in an outdoor chemical plant via a combination of LSTM-RNN and CFD simulation. Comput. Chem. Eng. 125, 476–489. https://doi.org/10.1016/j.compchemeng.2019.03.012.

Klise, K.A., Nicholson, B.L., Laird, C.D., Ravikumar, A.P., Brandt, A.R., 2020. Sensor placement optimization software applied to site-scale methane-emissions monitoring. J. Environ. Eng. 146 (7), 04020054. https://doi.org/10.1061/(asce)ee.1943-7870.0001737.

Kontos, Y.N., Kassandros, T., Perifanos, K., Karampasis, M., Katsifarakis, K.L., Karatzas, K., 2022. Machine learning for groundwater pollution source identification and monitoring network optimization. Neural Comput. Appl. 34 (22), 19515–19545. https://doi.org/10.1007/s00521-022-07507-8.

Lee, H., Lee, D., Lee, J., Shin, D., 2024. Efficient gas leak simulation surrogate modeling and super resolution for gas detector placement optimization. Comput. Chem. Eng. 181, 108508. https://doi.org/10.1016/j.compchemeng.2023.108508.

Legg, S.W., Benavides-Serrano, A.J., Siirola, J.D., Watson, J.P., Davis, S.G., Bratteteig, A., Laird, C.D., 2012. A stochastic programming approach for gas detector placement using CFD-based dispersion simulations. Comput. Chem. Eng. 47, 194–201. https://doi.org/10.1016/j.compchemeng.2012.05.010.

Li, T.Y., Zhou, J.F., Wu, C.C., Bao, L.J., Shi, L., Zeng, E.Y., 2018. Characteristics of polybrominated diphenyl ethers released from thermal treatment and open burning of E-waste. Environ. Sci. Technol. 52 (8), 4650–4657. https://doi.org/10.1021/acs.est.8b00780.

Liu, F., Wen, J.X., 2002. The effect of turbulence modelling on the CFD simulation of buoyant diffusion flames. Fire Saf. J. 37 (2), 125–150. https://doi.org/10.1016/S0379-7112(01)00022-4.

Liu, Y., Zhang, B., Mu, C., 2020. A comparative study of optimization models for the gas detector placement in process facilities. Comput. Chem. Eng. 143, 107095. https://doi.org/10.1016/j.compchemeng.2020.107095.

Lu, Y., Xu, Z., 2016. Precious metals recovery from waste printed circuit boards: a review for current status and perspective. Resour., Conserv. Recycl. 113, 28–39. https://doi.org/10.1016/j.resconrec.2016.05.007.

Lyu, S., Zhang, S., Huang, X., Peng, S., Yang, D., Sun, M., Qi, Q., 2023. CFD simulations of instantaneously released liquefied gas in urban areas: a case study of LPG tank truck accident in Wenling, China. Sustain. Cities Soc. 94, 104550. https://doi.org/10.1016/j.scs.2023.104550.

Ma, D., Gao, J., Zhang, Z., Zhao, H., 2021. Identifying atmospheric pollutant sources using a machine learning dispersion model and Markov chain Monte Carlo methods. Stochastic Environ. Res. Risk Assess. 35 (2), 271–286. https://doi.org/10.1007/s00477-021-01973-7.

Meteoblue. (2022). Simulated historical climate & weather data for Penang. In.

Neto, I.F.F., Sousa, C.A., Brito, M.S.C.A., Futuro, A.M., Soares, H.M.V.M, 2016. A simple and nearly-closed cycle process for recycling copper with high purity from end life printed circuit boards. Sep. Purif. Technol. 164, 19–27. https://doi.org/10.1016/j.seppur.2016.03.007.

OpenStreetMap, C. (2018). OpenStreetMap. In.

Opit, P.F., Kairupan, I.Y., Rusuh, F.M., 2021. A MILP model for water level sensor placement with multi-sensor and multi-disaster areas. Jurnal Teknik Industri 22 (2), 185–195.

Rad, A., Rashtchian, D., Badri, N., 2016. A risk based methodology for optimal placement of flammable gas detectors within open process plants. Process Saf. Environ. Protect. 105. https://doi.org/10.1016/j.psep.2016.10.012.

Şahin, Ü.A., Onat, B., Stakeeva, B., Ceran, T., Karim, P., 2012. PM10 concentrations and the size distribution of Cu and Fe-containing particles in Istanbul's subway system. Transport. Res. Part D: Transport Environ. 17 (1), 48–53. https://doi.org/10.1016/j.trd.2011.09.003.

Sahle-Demessie, E., Richardson, T., Han, C., Nrmrl, U.S., Dietrich, J., & Wang, J. (2017). Characterizing of emissions from open burning of electronic waste using TG-GC–MS system. In.

Shahabuddin, M., Uddin, M.N., Chowdhury, J.I., Ahmed, S.F., Uddin, M.N., Mofijur, M., Uddin, M.A., 2023. A review of the recent development, challenges, and opportunities of electronic waste (e-waste). Int. J. Environ. Sci. Technol. 20 (4), 4513–4520. https://doi.org/10.1007/s13762-022-04274-w.

Shumon, M.R.H., Ahmed, S., Islam, M.T., 2014. Electronic waste: present status and future perspectives of sustainable management practices in Malaysia. Environ. Earth Sci. 72 (7), 2239–2249. https://doi.org/10.1007/s12665-014-3129-5.

Stone, L., Hastie, D., Zigan, S., 2019. Using a coupled CFD – DPM approach to predict particle settling in a horizontal air stream. Adv. Powder Technol. 30 (4), 869–878. https://doi.org/10.1016/j.apt.2019.02.001.

Sun, L., Chen, X., Zhang, B., Mu, C., Zhou, C., 2020. Optimization of gas detector placement considering scenario probability and detector reliability in oil refinery installation. J. Loss. Prev. Process. Ind. 65, 104131. https://doi.org/10.1016/j.jlp.2020.104131.

Uzair, M., Jamil, N., 2020. Effects of hidden layers on the efficiency of neural networks. In: 2020 IEEE 23rd international multitopic conference (INMIC).

Wu, J., Liu, Z., Yuan, S., Cai, J., Hu, X., 2020. Source term estimation of natural gas leakage in utility tunnel by combining CFD and Bayesian inference method. J. Loss. Prev. Process. Ind. 68, 104328. https://doi.org/10.1016/j.jlp.2020.104328.

Xu, D., Chen, L., Zhan, W., Zhang, K., Lu, J., Ji, Y., Ma, R., 2023. Study on the leakage dispersion law of exposed high-pressure natural gas pipelines in the mountainous environment [Original Research]. Front. Energy Res. 10. https://doi.org/10.3389/fenrg.2022.1031006.

Xu, Q., Du, W., Xu, J., Dong, J., 2021a. Neural network-based source tracking of chemical leaks with obstacles. Chin. J. Chem. Eng. 33, 211–220. https://doi.org/10.1016/j.cjche.2020.12.022.

Xu, Y., Liu, X., Cao, X., Huang, C., Liu, E., Qian, S., Liu, X., Wu, Y., Dong, F., Qiu, C.-W., Qiu, J., Hua, K., Su, W., Wu, J., Xu, H., Han, Y., Fu, C., Yin, Z., Liu, M., Zhang, J., 2021b. Artificial intelligence: a powerful paradigm for scientific research. Innovation 2 (4), 100179. https://doi.org/10.1016/j.xinn.2021.100179.

Yakıcı, E., Karatas, M., 2021. Solving a multi-objective heterogeneous sensor network location problem with genetic algorithm. Comput. Netw. 192, 108041. https://doi.org/10.1016/j.comnet.2021.108041.

Yong, Y.S., Lim, Y.A., Ilankoon, I.M.S.K, 2019. An analysis of electronic waste management strategies and recycling operations in Malaysia: challenges and future prospects. J. Clean. Prod. 224, 151–166. https://doi.org/10.1016/j.jclepro.2019.03.205.

Yu, H.L., Chen, B.H., Kim, K.S., Siwayanan, P., Choong, S.Y.T., Ban, Z.H., 2022. Source localization for illegal plastic burning in Malaysia via CFD-ANN approach. Dig. Chem. Eng. 3, 100029. https://doi.org/10.1016/j.dche.2022.100029.

Zeng, L., Gao, J., Lv, L., Zhang, R., Chen, Y., Zhang, X., Huang, Z., Zhang, Z., 2020. Markov-chain-based inverse modeling to fast localize hazardous gaseous pollutant sources in buildings with ventilation systems. Build. Environ. 169, 106584. https://doi.org/10.1016/j.buildenv.2019.106584.

Zheng, J., Chen, K.H., Yan, X., Chen, S.J., Hu, G.C., Peng, X.W., Yuan, J.G., Mai, B.X., Yang, Z.Y., 2013. Heavy metals in food, house dust, and water from an e-waste recycling area in South China and the potential risk to human health. Ecotoxicol. Environ. Saf. 96, 205–212. https://doi.org/10.1016/j.ecoenv.2013.06.017.

Zheng, X., Chen, Z., 2010. Back-calculation of the strength and location of hazardous materials releases using the pattern search method. J. Hazard. Mater. 183 (1–3), 474–481. https://doi.org/10.1016/j.jhazmat.2010.07.048.

Zhou, X., 2021. Wireless sensor network deployment in cyberphysical machine tool system based on optimal allocation of memory buffers. J. Sens. 2021, 1–18.

Zhou, Z., Tartakovsky, D.M., 2021. Markov chain Monte Carlo with neural network surrogates: application to contaminant source identification. Stochastic Environ. Res. Risk Assess. 35 (3), 639–651. https://doi.org/10.1007/s00477-020-01888-9.